

## REVIEW

View Article Online  
View Journal | View Issue



Cite this: *Ind. Chem. Mater.*, 2025, 3, 311

# Catalyst design for ammonia decomposition: an overview

Tong Han,<sup>a</sup> Lu Wei,<sup>\*a</sup> Shaohua Xie,<sup>b</sup> Yuxi Liu,<sup>a</sup> Hongxing Dai <sup>a</sup> and Jiguang Deng <sup>\*a</sup>

Ammonia serves as a viable medium for hydrogen storage owing to its significant hydrogen content and elevated energy density, and the absence of carbon dioxide emissions during ammonia-to-hydrogen production has inspired more research on ammonia decomposition. Despite growing interest, a significant gap persists between the depth of existing studies and the practical approach to on-the-spot hydrogen generation using ammonia decomposition. The creation of effective and accessible catalysts to feed ammonia decomposition is a critical step in addressing this daunting challenge. This paper systematically summarizes four key catalyst design strategies, including size effect, alkalinity modulation, metal-support interactions, and alloying, informed by experimental and theoretical investigations into ammonia decomposition. Each strategy's underlying mechanism for enhancing ammonia decomposition is elucidated in detail. Moreover, the paper categorizes catalysts employed in existing ammonia decomposition reactors to guide future catalyst development. The influence of diverse energy sources and reactor configurations on catalyst performance is also discussed to provide a comprehensive framework for advancing ammonia decomposition catalyst research.

**Keywords:** Ammonia decomposition reaction; Catalyst design; Particle size effect; Adjustment of alkalinity; Strong metal-support interaction; Alloying effect.

Received 6th September 2024,  
Accepted 20th January 2025

DOI: 10.1039/d4im00112e

rsc.li/icm

## 1 Introduction

The pressing challenges of global energy and environmental pollution have motivated the international community to swiftly advance decarbonization efforts. The contradiction between the growing global energy demand and the escalating environmental impact has become more evident, which highlights the important global demand for clean and sustainable energy. To transition from fossil fuels to renewable energy and mitigate the effects of pollution emissions on the environment, green hydrogen energy serves as an essential component in the comprehensive decarbonization of the global energy system. As early as the mid-twentieth century, liquid ammonia has received widespread attention as a proven hydrogen energy carrier.<sup>1,2</sup> Ammonia possesses a substantial hydrogen content (17.6 wt%) and energy density (3 kW h kg<sup>-1</sup>) along with the capability to be stored and transported at room temperature

and 10 atmospheres. Furthermore, it is noteworthy that hydrogen production does not result in carbon dioxide emissions (Fig. 1a).<sup>3</sup> Therefore, the process of ammonia decomposition into hydrogen has garnered increased focus



Tong Han

*Tong Han is currently a PhD candidate major in Materials and Chemical Engineering at the College of Materials Science and Engineering, Beijing University of Technology. She has been actively engaged in groundbreaking research under the mentorship of Professor Jiguang Deng and Professor Lu Wei since 2023. Her research endeavors lie at the forefront of environmental catalysis, specifically focusing on the optimization of catalysts for*

*ammonia decomposition. This pivotal area of study holds immense potential for advancing sustainable energy technologies, as ammonia decomposition offers a promising route for hydrogen production. Her work exemplifies the intersection of materials science, chemistry, and environmental engineering.*

<sup>a</sup> Beijing Key Laboratory for Green Catalysis and Separation, Key Laboratory of Beijing on Regional Air Pollution Control, Key Laboratory of Advanced Functional Materials, Education Ministry of China, Beijing University of Technology, Beijing 100124, China. E-mail: weilu@bjut.edu.cn, jgdeng@bjut.edu.cn; Fax: +86 10 6739 1983; Tel: +86 10 6739 6118

<sup>b</sup> Department of Chemical and Environmental Engineering, University of California, Riverside, 900 University Ave, Riverside, CA 92521, USA



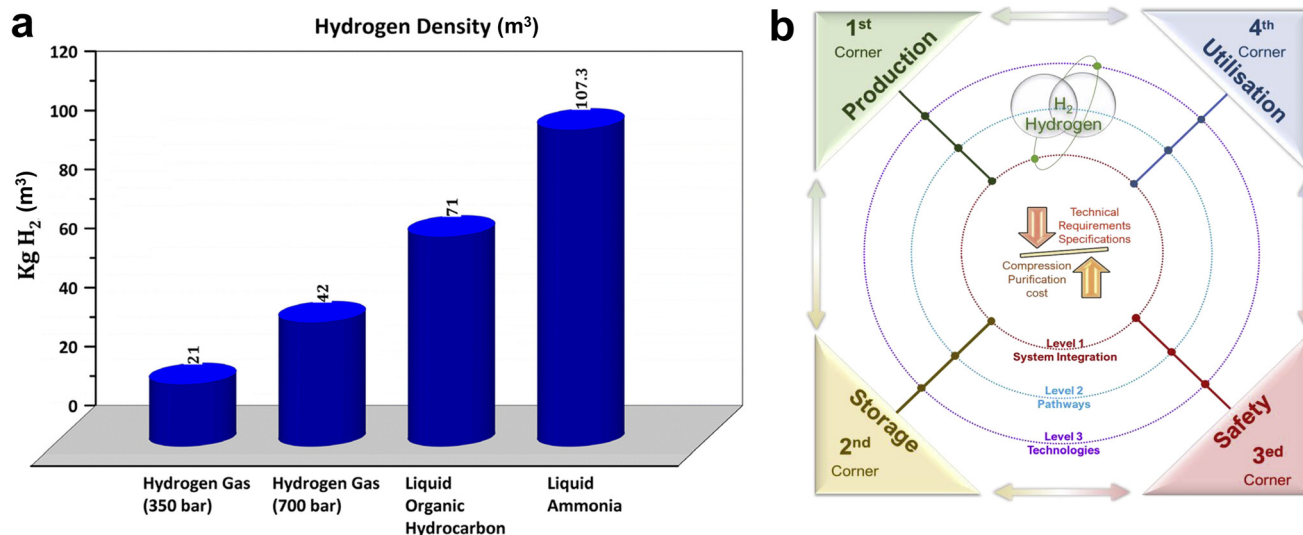


Fig. 1 (a) Density comparison of several kinds of hydrogen storage.<sup>3</sup> Copyright 2023, Royal Society of Chemistry. (b) The four-cornered model suggesting a hydrogen square.<sup>4</sup> Copyright 2020, Elsevier.

in recent years. The decomposition of ammonia presents a viable method for on-site hydrogen synthesis, successfully mitigating the significant problems associated with hydrogen shipping and storing that impede the broad adoption of the use of hydrogen (Fig. 1b).<sup>4</sup> Although the kinetics and mechanism of the ammonia decomposition reaction have been widely and deeply studied at an early stage, there is still no consensus on many important issues. In particular, the structure-sensitive nature of ammonia decomposition leads to different reaction mechanisms under varying conditions and catalysts, which seriously limits the continuous development, design, and application of the corresponding catalysts and reactors.

Ammonia decomposition, as a reversible process of the ammonia synthesis reaction, also shares common features in the application of catalysts. Nowadays, iron nitride,<sup>5</sup> Ru/CNT,<sup>6</sup> and Ni-CeO<sub>2</sub> (ref. 7) catalysts for ammonia synthesis by photo/electro/plasma catalysis at room temperature and ambient pressure are also relevant in the field of ammonia decomposition. Among them, the noble metal Ru-based catalysts are recognized as the optimal catalysts with high activity especially at low temperatures (below 500 °C).<sup>8</sup> Ru, the most studied element in ammonia decomposition catalysts, has been shown to achieve optimal exposure of B<sub>5</sub> sites with particle sizes ranging from 2 to 3 nanometers.<sup>9–11</sup> This finding underscores the significance of precise particle



Lu Wei

Dr. Lu Wei received his PhD in materials science and engineering from Beijing University of Technology in 2020. Afterwards, he worked as a Postdoctoral Fellow in the Department of Environmental Biology at Beijing University of Technology. He is currently an associate professor of Beijing University of Technology. He is the chair of the National Natural Science Foundation of China (NSFC) Youth Foundation and Postdoctoral Foundation. He

is mainly engaged in the research of novel catalyst design for catalytic applications in environmental chemistry. His research interests include quantitative calculations, first-principles calculations, molecular dynamics simulations, and in situ spectroscopic experiments in non-homogeneous phase catalysis.



Jiguang Deng

Dr. Jiguang Deng obtained his PhD degree from Beijing University of Technology in 2010. He is a full professor in the School of Materials Science and Engineering of Beijing University of Technology. He is also a member of the Environmental Chemistry Branch of the Chinese Society of Environmental Science, the Standing Committee of the Specialized Committee on VOCs Pollution Prevention and Control, and a technical expert

of the Exhaust Gas Purification Committee of the China Environmental Protection Industry Association. He is mainly engaged in the research on VOC pollution control and resource utilization as well as environmental catalysis chemistry.



size control in optimizing the reaction effectiveness in Ru-based materials towards ammonia decomposition. These types of catalyst design methods have a substantial influence on the catalytic performance of the target ammonia decomposition catalyst. Rational design of ammonia decomposition catalysts is one of the cornerstones to achieving efficient ammonia decomposition for hydrogen generation. However, the design and development of new ammonia decomposition catalysts have not been summarized in the literature.

In this review, several major catalyst design strategies are summarized from the perspective of catalyst design and development, including size effect, alkalinity modulation, metal-support interaction and alloy effect. The microscopic modulation mechanisms and mechanisms involved in each design strategy are also elaborated in detail. In addition, the applications of the catalysts in industrial reactors are also summarized. This review is intended to assist in the design and development of catalysts and reactors for hydrogen production from ammonia decomposition.

## 2 Ammonia decomposition catalysis technologies

Similar to ammonia synthesis technology, the catalytic technologies for ammonia decomposition mainly include thermal, photothermal, electrocatalytic, photoelectrocatalytic and microwave catalytic technologies. Among them, thermal catalysis is one of the many technologies widely studied because of its strong stability and industrialization basis. According to the results of the thermodynamic equilibrium theory of ammonia decomposition reaction, high temperature and low pressure are the necessary factors to realize the high decomposition rate of ammonia, which can reach 99% at 400 °C and ordinary pressure, but the temperature is as high as 700 °C if ammonia is to be completely decomposed.<sup>12</sup> In addition, due to the influence of external factors and the dynamic equilibrium of the

reaction, the actual thermal catalytic method to realize the ammonia decomposition process often requires higher temperatures. Therefore, the rationalization of ammonia decomposition catalysts will effectively improve the decomposition efficiency and reduce energy consumption. Gong *et al.* prepared a series of nickel-based catalysts based on zeolite Y with different cationic types and achieved 98%  $\text{NH}_3$  decomposition at 600 °C.<sup>13</sup> Han *et al.* used Co nanoparticles modified with dual structural constraints of  $\text{LaCoO}_x$  to achieve nearly 100% ammonia decomposition at 600 °C.<sup>14</sup> Whereas ruthenium-based catalysts tend to show better low-temperature catalytic activity than other ammonia decomposition catalysts, *e.g.*, Ru/CeO<sub>2</sub>NR achieves a decomposition of 91.29% at 450 °C, but it fails to achieve complete decomposition at 500 °C or even higher temperatures corresponding to decomposition greater than 99%.<sup>15</sup> Among the many literature reports, Fang *et al.* used Ru/MgO(111) to thermally catalyze ammonia decomposition, which can achieve full decomposition at about 450 °C (Fig. 2a and b),<sup>16</sup> which is the best performance achieved by a single thermally catalytic technology in the field of ammonia decomposition at present.

Typical microwave-assisted breakdown of ammonia with iron-based catalysts becomes analogous to the minimal degradation temperatures documented for thermal catalysis.<sup>18</sup> There is a growing interest in utilizing microwave field conditions to stimulate various catalysts to feed ammonia decomposition under lower temperatures. Through continuous refinement of the catalyst support and active components, a hybrid packing comprising Ni@Al<sub>2</sub>O<sub>3</sub>-carbon has achieved a remarkable decomposition efficiency of 99% at 400 °C in a pure ammonia stream.<sup>19</sup> Compared with conventional thermal catalysis, microwave catalysis can achieve significantly higher decomposition values due to selective heating and also provides an important basis for advancing the practical application of ammonia decomposition. In addition, the photothermal synergistic technology on SA-Co/CeO<sub>2</sub> catalysts showed ammonia

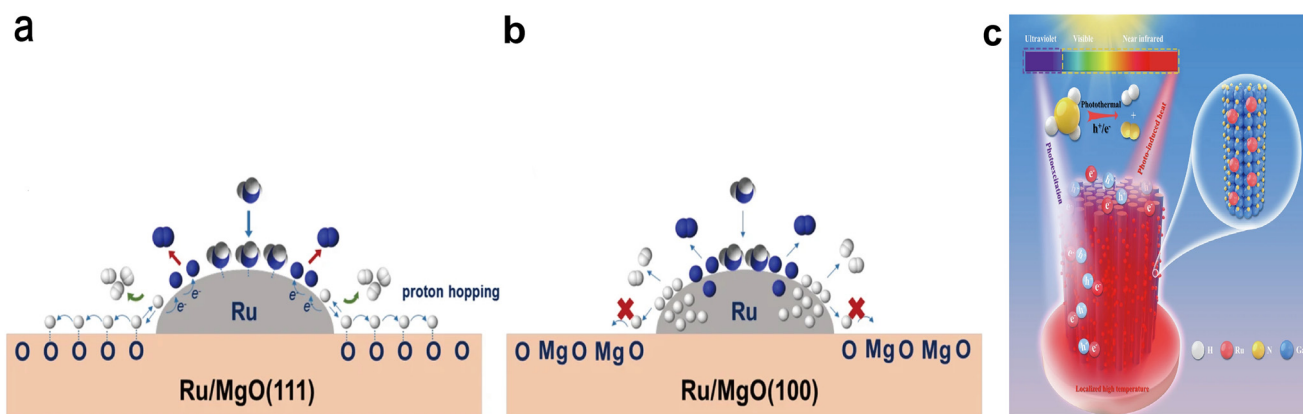


Fig. 2 Hydrogen diffusion over (a) Ru/MgO(111) and (b) Ru/MgO(100) exhibits distinct characteristics.<sup>16</sup> Copyright 2023, Nature Publishing Group. (c) Illustration of the cooperative action of charge carriers and photo-induced thermal energy in accelerating the removal of ammonia on Ru NPs/GaN NWs/Si.<sup>17</sup> Copyright 2024, Nature Publishing Group.



decomposition performance with a  $\text{H}_2$  production rate of  $29.1 \text{ mmol g}^{-1} \text{ min}^{-1}$  at  $450^\circ\text{C}$ .<sup>20</sup> Li *et al.* demonstrated that  $0.15 \text{ mmol cm}^{-2} \text{ h}^{-1}$  hydrogen was produced at  $270^\circ\text{C}$  under natural light irradiation and an external heating system (Fig. 2c).<sup>17</sup> Existing photothermal synergistic technologies use a certain mass fraction of ammonia solution as the ammonia feedstock, so there is still much room for development in the estimation of the actual decomposition rate and subsequent applications.

Ammonia decomposition technologies related to electrocatalysis are broadly divided into two directions: the advancement of ammonia decomposition in conjunction with fuel cells and the development of more efficient low-temperature catalytic methods. Ammonia-fueled solid oxide fuel cells (SOFCs) can achieve more than 90% ammonia decomposition at temperatures above  $700^\circ\text{C}$ .<sup>21</sup> The  $\text{NH}_3$  decomposition rates of four low-cost metals as SOFC anodes were investigated by Zheng *et al.*<sup>22</sup> Lim and colleagues employed Cs enhanced Ru/CNT as a thermal decomposition catalyst to build  $\text{CsH}_2\text{PO}_4$  mixed on carbon black into an electrochemical cell, obtaining a hydrogen generation rate of  $1.48 \text{ mol}_{\text{H}_2} \text{ g}_{\text{cat}}^{-1} \text{ h}^{-1}$  at  $0.4 \text{ V}$  bias and  $250^\circ\text{C}$ .<sup>23</sup> SOFCs applied to  $\text{NH}_3$  decomposition will facilitate faster achievement of ammonia-hydrogen hybrid engine goals. Łuczak *et al.* achieved a hydrogen production rate of  $6.2 \text{ kg}_{\text{H}_2} 100 \text{ kg}^{-1}$  solution at  $20^\circ\text{C}$  by electrocatalytic ammonia decomposition using a nickel-based catalyst.<sup>24</sup> Džibelová *et al.* demonstrated that 2D hexagonal ferrite alloys impregnated with Ru can absorb visible light and synergize electrochemical properties to achieve a small amount of hydrogen production from  $\text{NH}_3$  decomposition at  $24^\circ\text{C}$ .<sup>25</sup> These results show a trend toward lower temperature and even room temperature for ammonia decomposition, but how to maintain an efficient hydrogen production rate at lower temperature remains a difficulty to address. Because different catalytic technologies transfer energy in different ways, their catalyst types and catalytic efficacy are also different (see Table 1 for a full comparison). Either way, the advancement will be more favorable to the practical application of ammonia decomposition.

### 3 Theoretical studies on ammonia decomposition

In order to promote the development of ammonia decomposition, relevant basic theoretical research is

indispensable. However, different catalytic technologies and catalysts have important influences on the catalytic process of ammonia decomposition, and thus a completely unified mechanism of ammonia decomposition has yet to be formed. For photocatalytic and electrocatalytic technologies, the existing studies have used aqueous ammonia solution as the ammonia source, and supplemented with NaOH and other modifiers to participate in the decomposition reaction, which makes the intermediate process of the reaction more complicated and the study of the mechanism more difficult. On the other hand, thermal catalytic technology, as a relatively stable and mature technology in the field of ammonia decomposition, involves only a gas-solid reaction in the reaction process, which also better reflects the reaction characteristics of  $\text{NH}_3$ . Therefore, we will focus on the theoretical study of thermally catalyzed ammonia decomposition.

#### 3.1 Mechanism of ammonia decomposition

Thermally catalyzed  $\text{NH}_3$  decomposition for hydrogen generation exemplifies the reaction characteristics associated with ammonia decomposition, which is a relatively simple reaction system with weak overall heat uptake and volume increase. Recent research indicates an amount of  $\text{H}_2$  suppresses the process. Hence, the reactivity rate is contingent upon the concentrations of ammonia and hydrogen.<sup>26</sup> However, since the kinetics of the single-step reaction varies with the reaction factors, including reaction temperature, reactant coverage across the catalyst surface, and overall catalyst itself, the rate-controlling step of the reaction also varies with the reaction conditions.<sup>27</sup> At present, two primary mechanistic models, Tamaru and Temkin-Pyzhev, were developed for ammonia decomposition processes.

The Tamaru mechanism was obtained under the assumption that  $\text{NH}_3$  adsorption and  $\text{N}_2$  desorption are jointly the rate-controlling steps of the reaction, and the reaction rate equation was obtained as:<sup>28</sup>

$$r = k p_{\text{NH}_3}^\alpha k p_{\text{H}_2}^\beta k p_{\text{N}_2}^\gamma \quad (1)$$

where  $\alpha$ ,  $\beta$  and  $\gamma$  represent the numbers of reaction stages ( $\alpha > 0$ ,  $\beta$  and  $\gamma < 0$ ),  $k$  is the reaction rate constant, and  $P_{\text{NH}_3}$ ,  $P_{\text{H}_2}$  and  $P_{\text{N}_2}$  are the partial pressures of  $\text{NH}_3$ ,  $\text{H}_2$  and  $\text{N}_2$ , respectively. Normally the reaction is a zero-level reaction for

**Table 1** Summary of different technologies and ammonia decomposition performance

| Catalysis technology type | Catalyst                     | Catalyst support | Reaction temperature ( $^\circ\text{C}$ ) | $\text{NH}_3$ conversion (%) | $\text{H}_2$ production                                    | Ref. |
|---------------------------|------------------------------|------------------|---|------------------------------|--|------|
| Thermal                   | Ni-based catalysts           | Zeolite Y        | 600                                       | 98                           | —  | 13   |
|                           | Ru-based catalyst            | $\text{CeO}_2$   | 450                                       | 91                           | —  | 15   |
|                           |                              | $\text{MgO}$     | 450                                       | 100                          | —  | 16   |
| Microwave                 | $\text{Ni@Al}_2\text{O}_3$   | Carbon           | 400                                       | 99                           | —  | 19   |
| Photothermal              | Ru NPs/GaN                   | NWs/Si           | 270                                       | —                            | $0.15 \text{ mmol cm}^{-2} \text{ h}^{-1}$                 | 17   |
| Electrochemical           | Ni-Cu catalyst               | Nickel felt      | 20  | —                            | $6.2 \text{ kg}_{\text{H}_2} 100 \text{ kg}^{-1}$ solution | 24   |
| Photoelectrochemical      | $\text{RuO}_2$ nanoparticles | 2D hematene      | 24  | —                            | $\sim 28 \text{ mmol H}_2 \text{ mg}^{-1}$                 | 25   |





$N_2$  and  $H_2$ , so the reaction rate is related only to the partial pressure of ammonia and the reaction rate equation can be written as:

$$r = k p_{NH_3}^\alpha \quad (2)$$

The Temkin-Pyzhev mechanism posits that nitrogen atom binding desorption is the controlling step, and the resulting kinetic expression for the reaction rate is:<sup>29</sup>

$$r = k \left[ \left( \frac{p_{NH_3}^2}{p_{H_2}^3} \right)^\beta - \frac{p_{N_2}}{k_{ep}^2} \left( \frac{p_{H_2}^3}{p_{NH_3}^2} \right)^{1-\beta} \right] \quad (3)$$

The reaction constant  $k$  can be estimated using the Arrhenius equation:

$$k = k_0 \times e^{-E_a/RT} \quad (4)$$

where  $r$  is the reaction rate,  $k$  is the reaction rate constant,  $P_{NH_3}$ ,  $P_{H_2}$ , and  $P_{N_2}$  are the partial pressures of  $NH_3$ ,  $H_2$ , and  $N_2$ , respectively;  $\beta$  is a constant related to the surface of the catalyst,  $k_0$  and  $E_a$  are the pre-exponential factor and the activation energy, respectively;  $R$  is the gas constant ( $8.314 \text{ kJ mol}^{-1} \text{ K}^{-1}$ ), and  $T$  is the reaction temperature.

The first term in eqn (3) is the rate of the  $NH_3$  decomposition reaction, with  $N_2$  exerting no influence on the reaction, so the effect of  $N_2$  partial pressure can be ignored; the subsequent term denotes the rate of ammonia synthesis, which occurs minimally and thus may be neglected.

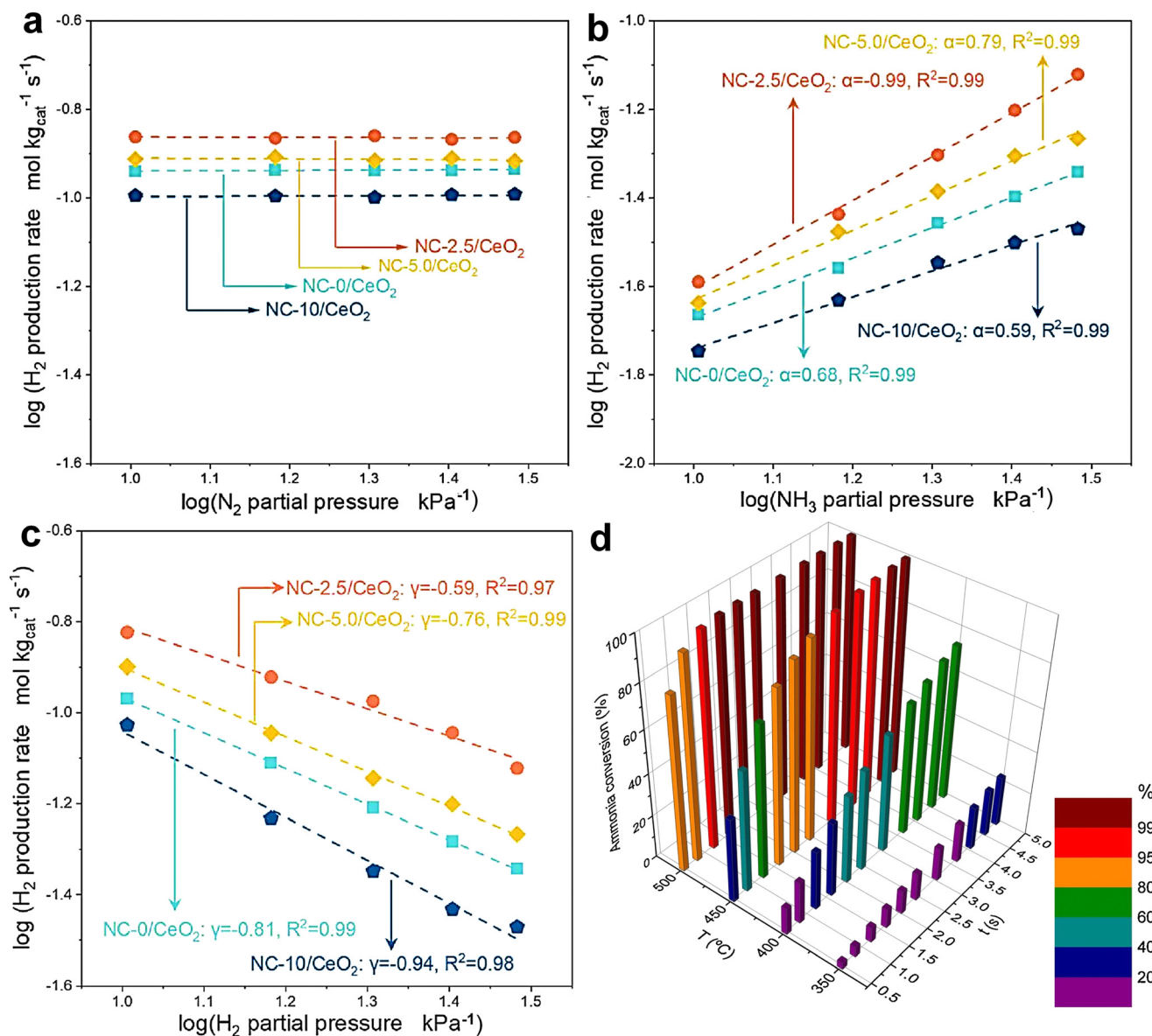


**Fig. 3** Determining the exact order of reaction for (a)  $N_2$ , (b)  $NH_3$ , and (c)  $H_2$  using kinetics graphs.<sup>31</sup> Copyright 2023, Elsevier. (d) Results from a mathematical model of ammonia decomposition on 2.5Ni0.5Ru/CeO<sub>2</sub> under different temperatures and interaction periods with dry ammonia.<sup>32</sup> Copyright 2021, Elsevier.



Consequently, the Temkin–Pyzhev model is able simplified toward the following equation:<sup>30</sup>

$$r = k_0 \exp\left(\frac{-E_a}{RT}\right) p_{\text{NH}_3}^\alpha p_{\text{H}_2}^\beta (\alpha > 0, \beta < 0) \quad (5)$$

where  $\alpha$  and  $\beta$  are the reaction levels of  $\text{NH}_3$  and  $\text{H}_2$ , respectively, where the reaction level of  $\text{H}_2$  is negative, indicating that  $\text{H}_2$  inhibits the ammonia decomposition reaction.

He *et al.* developed a bimetallic  $\text{Ni}_x\text{Co}_{10-x}/\text{CeO}_2$  ammonia decomposition catalyst suitable for medium temperatures (700 °C), and their kinetic studies showed that the ammonia decomposition reaction on the catalyst's surface followed the Temkin–Pyzhev mechanism, and the related kinetic calculations are shown in Fig. 3a–c.<sup>31</sup>

However, the actual reaction mechanism during  $\text{NH}_3$  decomposition for hydrogen production still cannot be fully elucidated by a particular mechanism. Oyama<sup>33</sup> investigated the kinetic mechanism of the ammonia decomposition reaction on vanadium nitride, noting that the kinetic variations were attributed to the switch of the Temkin–Pyzhev mechanism to the Tamar mechanism with increasing temperature. Lucentini showed that the adsorbed ammonia dehydrogenation reaction constituted the rate-controlling step of the ammonia decomposition process on  $\text{Ni-Ru/CeO}_2$  by using a kinetic model for evaluating the hydrogen generation rate across various operating conditions (the corresponding calculations correspond to Fig. 3d).<sup>32</sup> A lot of literature explores the influence of various ammonia decomposition catalysts (including supports and promoters) and reaction factors (such as temperature and pressure) on reaction kinetics<sup>34–36</sup> and indicates that the decomposition is influenced by reaction temperature and reactant surface species, which poses a challenge to the development of related catalysts and reactors.

### 3.2 Theoretical calculations reveal ammonia decomposition

Ammonia synthesis catalysts are often referenced in the design of  $\text{NH}_3$  decomposition materials. However, highly active ammonia decomposition catalysts are not correlated to the best ammonia synthesis catalysts. Consequently, the creation of high-performance ammonia decomposition catalysts is inevitably dependent on the theoretical calculations that shed light on the reaction mechanism. Logadottir and others proposed a methodology to explain the movement between ammonia synthesis catalysts' ability and transition metal catalysts.<sup>37</sup> Because the equilibrium state for its primary surface components and the activation energy of the rate-controlling step are determined by the free chemisorption energy, which has a linear relation *via* the Brønsted–Evans–Polanyi connection, the metal's activity in ammonia synthesis is determined by this energy. Since the model is in line with the microscopic reversibility principle, it might have been utilized to analyze the ammonia decomposition trend at concentrations higher than the equilibrium value. For ammonia production and ammonia decomposition circumstances, Fig. 4a shows the trend forecasts (volcano curves) based on this model.<sup>38</sup> To further demonstrate the model's applicability to ammonia decomposition reactions, kinetic checks were performed experimentally and theoretically by calculating the kinetics of the reaction in combination with different ammonia decomposition catalysts. These findings obtained from calculations based on density functional theory (DFT) are presented in Fig. 4b. The results obtained from DFT calculations were plotted as a function of ammonia decomposition rate and nitrogen binding energy for different monometallics.<sup>39</sup> The volcano plots show that ruthenium metal has the best performance. In contrast to the volcano curves used for ammonia synthesis, the best decomposition

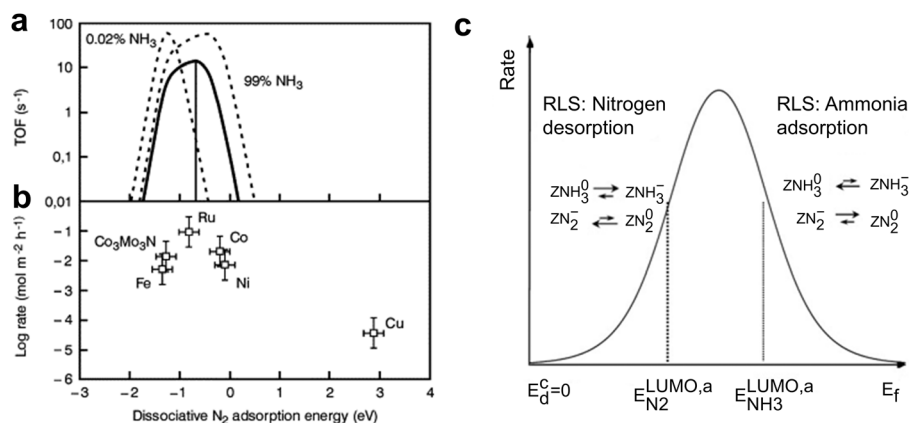


**Fig. 4** (a) The ammonia decomposition turnover frequency is depicted as a function of the free  $\text{N}_2$  adsorption reaction energy at 0.02, 20 (dashed line), and 99% decomposition at circumstances of 773 K, 1 bar, and a 3 : 1  $\text{H}_2/\text{N}_2$  ratio. (b) Rates of ammonia decomposition were experimentally determined for different catalysts at a temperature of 773 K, with a pressure of 1 bar, a hydrogen-to-nitrogen ratio of 3 : 1, and an ammonia concentration set at 20%.<sup>38</sup> Copyright 2005, Elsevier. (c) An arbitrary metal catalyst's Fermi level in relation to the ammonia decomposition reaction rate. On each side of the rate maximum are the antibonding LUMOs of ammonia and nitrogen species that have been adsorbed. The rate-limiting step is RLS.<sup>41</sup> Re-drawing from ref. 41. Copyright 2020, American Chemical Society.



catalysts are those with weaker nitrogen binding, and similarly, the optimal position for the volcano curves in  $\text{NH}_3$  decomposition is significantly influenced by the reaction circumstances. In addition, it can be seen that it is necessary to employ catalysts of different nitrogen binding energies toward optimum ammonia decomposition.<sup>40</sup> The theoretical and computational studies establish a foundation for continued in-depth investigation of  $\text{NH}_3$  decomposition reactions and the design of their corresponding catalysts.

The literature identifies two potential rate-limiting steps in ammonia decomposition:  $\text{NH}_3$  adsorption and  $\text{N}_2$  desorption, both affected by the catalyst's metal composition and process parameters.<sup>42</sup> The  $\text{N}_2$  desorption step is the one that limits the rate at low temperatures.<sup>43</sup> Based on this, when designing a catalyst for ammonia decomposition, the right metal-N-binding energy is a crucial factor.<sup>44</sup> The equilibrium fraction of the adsorbed material in various chemisorption states is contingent upon the energy differential caused by the Fermi level of the catalyst and the antibonding LUMOs of the adsorbate. The reaction rate demonstrates the correlation between the Fermi level and the volcanic profile. The rivalry among the exponential term of the catalyst Fermi level separation and the antibonding LUMO of adsorbed  $\text{NH}_3$  and  $\text{N}_2$  is illustrated by the volcano profile of the Fermi levels across several metals. Fig. 4c provides a simple illustration; a downward shift of the Fermi level traversing the antibonding LUMO of ammonia favors strong adsorption of ammonia molecules, whereas an upward trend approaching the antibonding LUMO of  $\text{N}_2$  promotes the desorption of neutral  $\text{ZN}_2^0$  species.<sup>41</sup> Obviously, the Fermi energy level alignment of the catalyst is optimal amid the antibonding LUMO state of  $\text{NH}_3$  and  $\text{N}_2$  adsorbed species. This location can anticipate the rate-determining step and the predominant surface species; the left side of the center leads to the constraint in  $\text{N}_2$  desorption, while the right side of the center points to the limitation in  $\text{NH}_3$  adsorption. It aligns with the traditional qualitative Sabatier

principle and the quantitative theoretical findings about optimum binding energy suggested by Nørskov and associates.<sup>45</sup>

With the continuous improvement of theoretical models, more and more studies have been conducted to reveal the reaction mechanism of  $\text{NH}_3$  decomposition on specific catalysts using theoretical calculations. Duan *et al.* thoroughly examined the reaction mechanism of  $\text{NH}_3$  decomposition on the close-packed surfaces of late 3d transition metals, utilizing DFT as the primary theoretical tool. This investigation specifically focused on the Fe(110), Co(111), and Ni(111) surfaces, where they determined the adsorption geometries and corresponding adsorption energies of the intermediates involved in the  $\text{NH}_3$  decomposition process. The precise configuration of these intermediates and their energetic interactions with the surfaces are illustrated schematically in Fig. 5a, providing a clear visual representation of the underlying chemical phenomena.<sup>46</sup> Fang *et al.* demonstrated through a combination of experiments and DFT calculations that Ru on polar MgO(111) has a strong metal-carrier interaction that inhibits hydrogen poisoning of the Ru surface during ammonia decomposition, leading to better heterolytic  $\text{NH}_3$  activation and facilitating N-N recombination (as shown in Fig. 5b), with a catalytic activity that is at least four times higher than that of the (100) and (110) surfaces at a low temperature of 450 °C.<sup>16</sup> Notably, this supported surface can produce atomically dispersed Ru, which outperforms Ru nanoparticles in  $\text{NH}_3$  decomposition. Pathak and colleagues thoroughly elucidated the electronic nature of the catalyst through rigorous first-principles calculations involving Bader charge, density of state (DOS), and crystal orbital Hamiltonian population (COHP) calculations. Their findings revealed that the incorporation of Mo dopants onto the surface of  $\text{Fe}_3\text{N}(111)$  results in a notable transfer of electrons to the surface, thereby profoundly modifying the overall electronic landscape of the catalytic material. This

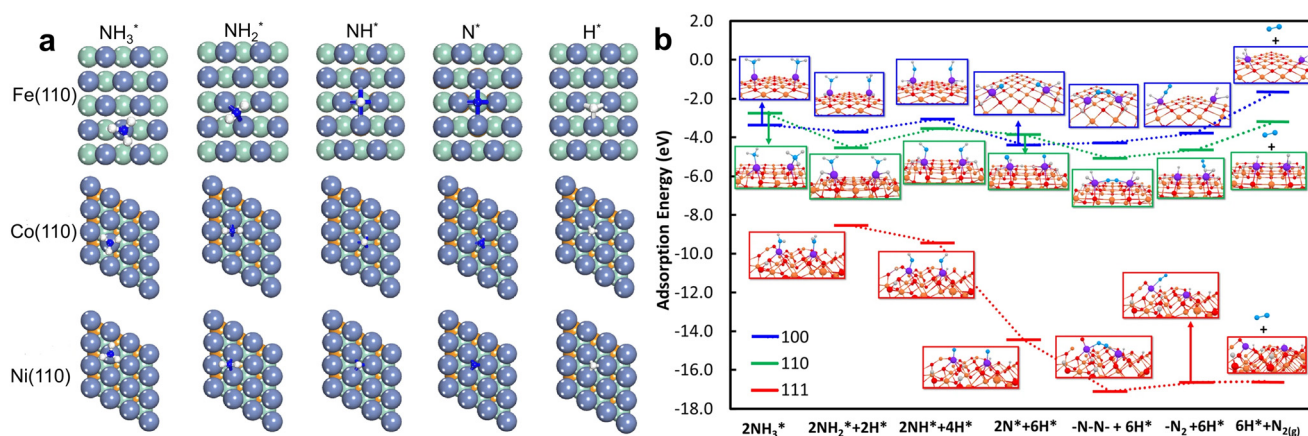


**Fig. 5** (a) Fe(110), Co(111) and Ni(111) surfaces exhibit the most stable  $\text{NH}_x$  ( $x = 0-3$ ) and H adsorption arrangements.<sup>46</sup> Re-drawing from ref. 46. Copyright 2012, Elsevier. (b) At MgO-supported twin Ru single atoms, energy patterns and their related optimized intermediate structures for ammonia decomposition and N-N recombination routes to generate  $\text{N}_2$  are shown.<sup>16</sup> Copyright 2023, Nature Publishing Group.





comprehensive investigation provides a deep understanding of the electronic interactions and structural modifications induced by Mo doping, offering valuable insights into the catalytic performance and potential of the modified  $\text{Fe}_3\text{N}$  system. The activation energy of the intermediate step of  $\text{NH}_3$  decomposition on the Mo-doped  $\text{Fe}_3\text{N}$  surface is greatly reduced compared with that of the undoped  $\text{Fe}_3\text{N}$ .<sup>47</sup> Combined with theoretical calculations, the effect of the microscopic changes on the catalyst surface and the rapid control step on the overall reaction rate of the ammonia decomposition reaction can be further clarified, which also provides guidance for the rational and effective design and development of ammonia decomposition catalysts.

## 4 Design of ammonia decomposition catalysts

Based on the above characteristics of the  $\text{NH}_3$  decomposition reaction, how to design and develop efficient ammonia decomposition catalysts has become one of the urgent problems. The existing catalysts for ammonia decomposition are summarized and sorted out, which can be roughly classified into four main catalyst design strategies: size effect, alkalinity modulation, metal-support interaction, and alloy effect (Fig. 6). The following subsections are a detailed description of each strategy in the context of the existing literature.

### 4.1 Particle size effect

It is widely acknowledged that the decomposition of ammonia is a microstructure-dependent reaction, wherein extensive experimental and theoretical investigations have

elucidated the pivotal roles played by the particle sizes of both the metallic active phase and the supporting carrier in modulating the kinetics and mechanisms of the  $\text{NH}_3$  decomposition process.<sup>48,49</sup> As the most active metal in the  $\text{NH}_3$  decomposition process, Ru has been experimentally and theoretically demonstrated to have a size effect, with the Ru  $\text{B}_5$ -type site being the main active site and the Ru size being no larger than 5 nm (generally 2–3 nm is dominant).<sup>50</sup> For the transition metal Fe, it has also been demonstrated that smaller particle sizes are favorable for aminolysis.<sup>51</sup> For the transition metal Ni, it has been demonstrated that smaller particle sizes are favorable for ammonia decomposition, and DFT calculations have consistently verified the existence of a close relationship between the particle size and the reactivity of transition metals (Fig. 7f).<sup>52</sup> In addition, there are relevant theoretical and experimental studies reporting the size effect of multicomponent nanoparticles of commonly used transition metals, such as NiCo, FeMo, CoMo, *etc.*<sup>53</sup>

Not only that, the morphology and size of the carrier also bring significant effects on the overall activity of  $\text{NH}_3$  decomposition catalysts.<sup>57</sup> Specifically, when  $\text{MgAl}_2\text{O}_4$  is utilized as the carrier, the reduced particle size of Ru on Ru/ $\text{MgAl}_2\text{O}_4$  significantly enhances the exposure of the  $\text{B}_5$  site of Ru, thereby favoring catalytic activity (Fig. 7a and b).<sup>54</sup> Furthermore, the utilization of the ion exchange method for depositing nano- and sub-nano-sized Ru particles within molecular sieves with precisely designed pore size structures results in size-controlled Ru particles that demonstrate exceptional catalytic activity (Fig. 7e).<sup>56</sup> Additionally, confining Ru within the 13X zeolite structure further amplifies its catalytic performance.<sup>58</sup> In parallel, experimental studies on microencapsulated reactions involving nanoparticles encapsulated in a Ni–Ru core-shell structure have also highlighted the influence of carrier morphology on the size effect, emphasizing the significance of these factors in optimizing catalytic performance.<sup>59</sup> The same size effect was observed in transition metal oxides when employed as stand-alone catalysts. For instance, alumina particles with a size of 1  $\mu\text{m}$  exhibited a larger surface area, leading to an increased residence time for ammonia decomposition, thereby enhancing catalytic performance (Fig. 7c and d).<sup>55</sup> The size effect in the design of ammonia decomposition catalysts converges the two key strategies of spatially confining domains and crafting interfaces. Moreover, it offers a pivotal reference point for the design and innovation of analogous catalysts tailored for the catalysis of small-molecule gases, thereby advancing the field towards more efficient and targeted catalysis.

### 4.2 Adjustment of alkalinity

Alkalinity enhancement of a material's surface can often help to enhance its ability to donate electrons. Therefore, increasing the surface alkalinity of catalysts is beneficial to modulate the electronic states around their reactive centers. The most typical method for modulating the surface

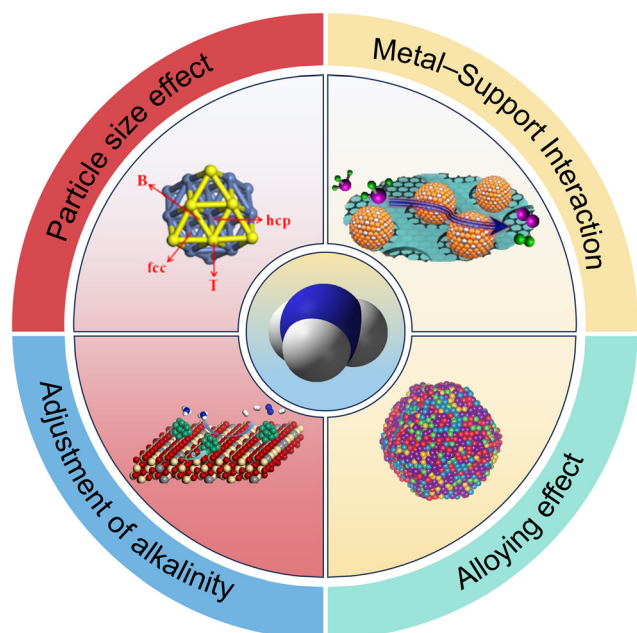
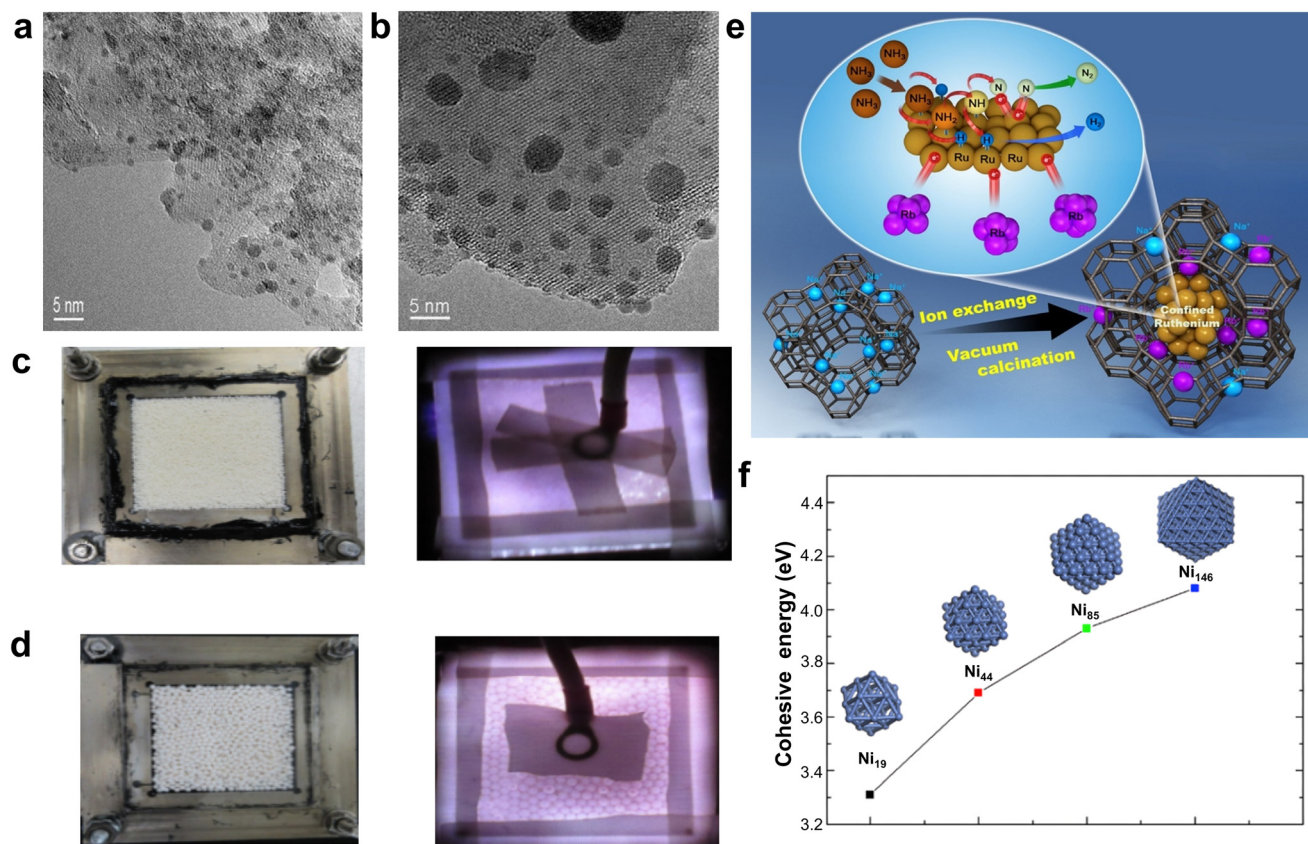


Fig. 6 Design strategies for ammonia decomposition catalysts.







**Fig. 7** (a) Ru/MgAl<sub>2</sub>O<sub>4</sub> and (b) Ru/Si<sub>3</sub>N<sub>4</sub> are shown in TEM pictures.<sup>54</sup> Copyright 2000, Elsevier. Images of the catalytic reactor featuring alumina: (c) the particle dimension of Al<sub>2</sub>O<sub>3</sub> is 1 mm, (d) the particle dimension of Al<sub>2</sub>O<sub>3</sub> is 2 mm.<sup>55</sup> Copyright 2020, Elsevier. (e) Diagram showing extremely monodisperse nano- and sub-nano-Ru particles trapped in base-exchanged zeolite Y.<sup>56</sup> Copyright 2021, Elsevier. (f) The Ni<sub>19</sub>, Ni<sub>44</sub>, Ni<sub>85</sub> and Ni<sub>146</sub> nanoclusters' most stable combinations and the stability of those configurations.<sup>52</sup> Re-drawing from ref. 52. Copyright 2017, Elsevier.

alkalinity of ammonia decomposition catalysts is alkaline doping. Among them, the most commonly used are alkali metals (Li, K, Cs, *etc.*), which are widely recognized as basic promoters for NH<sub>3</sub> decomposition catalysts due to their ability to facilitate product desorption.<sup>60,61</sup> At the same time, they are also effective adjuvants to prevent the sintering of Ru or Fe.<sup>62,63</sup> Whether it is loaded catalysts or one-piece catalysts, alkaline doping effectively enhances the overall catalytic activity of the catalysts.<sup>60</sup> In the context of Ru-based

supported catalysts, a prevalent approach in the literature involves doping the carrier with alkali and alkaline earth metals to enhance the alkalinity of the catalyst surface in contact with NH<sub>3</sub>, thereby affecting the complex desorption kinetics of the nitrogen atoms on the surface<sup>64</sup> and accelerating the process of the N atoms coming out of the surface of the catalyst.<sup>65</sup> As for the monolithic catalysts, few studies have been reported. Recently, it has been demonstrated that doping typical alkali metal Na into Co<sub>3</sub>O<sub>4</sub>

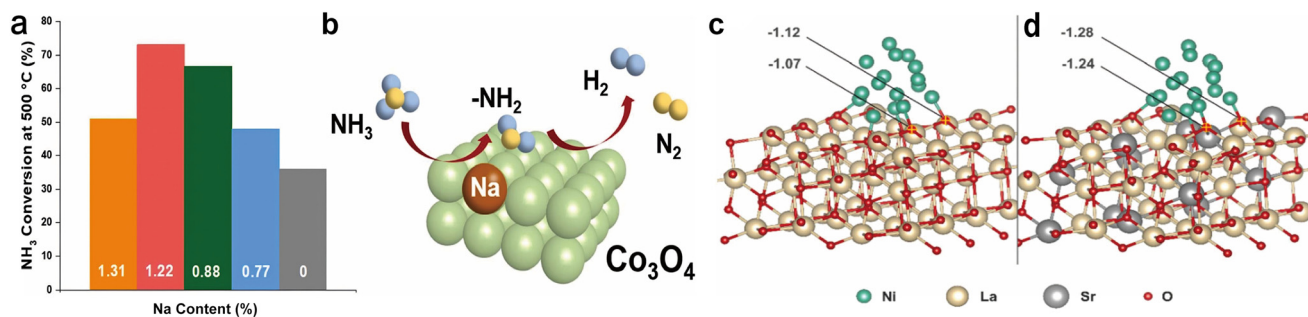


**Fig. 8** (a) Comparison of ammonia decomposition rates *via* Na-doped Co<sub>3</sub>O<sub>4</sub> and Co<sub>3</sub>O<sub>4</sub>-CA. (b) Diagrammatic representation of the catalyst surface ammonia decomposition process.<sup>66</sup> Copyright 2023, Elsevier. Ni/La<sub>2</sub>O<sub>3</sub> (c) and Ni/Sr-La<sub>2</sub>O<sub>3</sub> (d) structural models and Hirshfeld charge of multiple O atoms.<sup>67</sup> Copyright 2020, Elsevier.



catalysts with different ratios can also significantly enhance their catalytic activities, with the best catalysts showing an activity enhancement of about 20% compared with single  $\text{Co}_3\text{O}_4$  catalysts (Fig. 8a and b).<sup>66</sup>

In addition to the well-known alkali or rare earth metals, their related compounds also have a wide range of applications in ammonia decomposition (Fig. 8c and d).<sup>67</sup> The promotion of ammonia decomposition over Ru-based catalysts has been reported by a series of alkali metal amides, and the order of their activities was  $\text{Ru}-\text{Ba}(\text{NH}_2)_2 > \text{Ru}-\text{Ca}(\text{NH}_2)_2 > \text{Ru}-\text{Mg}(\text{NH}_2)_2$ , which showed that alkaline earth metal amides provided the  $\text{NH}_x$ -rich environment to facilitate the coupling of  $\text{NH}_x$  adsorbed on Ru to release  $\text{N}_2$  and  $\text{H}_2$ .<sup>68</sup> The incorporation of alkali hydroxides and the subsequent *in situ* formation of alkali aluminates during the synthesis of ammonia decomposition catalysts with supported active sites constitute a pivotal modification to the carrier material. This modification can be harnessed to significantly enhance the overall catalytic activity, achieving an improvement factor of up to 6.5 times compared to the pristine catalyst.<sup>69</sup> In addition, there is a cycling facilitation effect between the related nitrides and hydrides and transition metals.<sup>70</sup> The use of vanadium as a catalyst for  $\text{NH}_3$  decomposition has been shown to be a significant contributor to the development of the  $\text{NH}_x$ -rich environment in Ru. In the case of vanadium, for example, it can be inferred that the 3d state of vanadium strongly interacts with the 2p state of carbon, thereby altering the electron density at the Fermi energy level and forming an electronic structure similar to that of the noble metals. Typically, the C and N in the metal carbides and metal nitrides occupy interstitial sites between the larger metal atoms, thereby altering the electronic properties of the surface and thereby reducing the surface ammonia decomposition activation energy.<sup>8</sup> Taken together, it can be hypothesized that regulating the alkalinity of the catalyst surface is primarily a way to modulate the microenvironment around the reaction sites of the catalyst, thereby improving performance.

### 4.3 Metal-support interaction

Most studies have shown that moderate N-H binding strength and nitrogen desorption are essential for promoting  $\text{NH}_3$  decomposition.<sup>71</sup> To augment the population of electron donors available to the active metal site, thereby intricately modulating the pivotal N-N bond, and given the ubiquitous utilization of supported catalysts in ammonia decomposition reactions, the metal-support interactions emerge as a pivotal strategy. This can be achieved by strategically selecting different carrier materials and subsequently optimizing the dispersion of metal particles on the carrier surface to construct optimal interfaces for catalytic enhancement. Metal-support interaction is considered to be the key to controlling the reducibility, and it also accelerates the electrical charge jump between the active metal particles and

the support, which improves the activity and durability effects of the support and promoter.<sup>72</sup>

It has been reported that the chemical state of ruthenium in loaded catalysts is determined by interactions with the carrier and promoter, and that a carrier with higher electronegativity will stabilize the oxidation state of ruthenium to a greater extent thereby contributing to the reduction of its catalytic activity.<sup>73</sup> Therefore, the ideal carrier should have a high surface area, low electronegativity, and excellent thermal and chemical stability.<sup>74</sup> The electronegativity of carbon is less than that of the conventional carrier alumina, and the Ru/C catalyst is correspondingly more active than the classical catalyst Ru/ $\text{Al}_2\text{O}_3$ .<sup>75</sup> Due to its superior electrical conductivity and remarkable specific surface area, the carbon-based material enhances electron transfer to the Ru active site, thereby serving as an outstanding catalytic support for ammonia decomposition.<sup>76</sup> Different carbon carrier materials have different effects on the catalytic activity of Ru-based catalysts. For example, carbon nanotubes (CNTs) as the carrier of Ru catalysts showed good performance; N doping into carbon improved the metal-N bond strength, providing more active sites for N single bonding, H-bond cleavage, and N conjugation desorption, and thus improved the catalytic activity.<sup>77</sup> At the same time, because of the high dispersibility of the Ru particles and the high electronic conductivity of the carbon-based carriers, it is possible to change the electronic state of the Ru particles.<sup>78</sup> The catalytic activities of Ru-based catalysts were also affected by different carbon carriers. Graphene oxide obtained by the pre-reduction of graphene (GO) with 2-chloroethylamine hydrochloride has a more favorable electronic conductivity and higher alkalinity, which promotes the catalytic stability of the catalyst.<sup>79</sup> Porous silicon carbide ( $\beta$ -SiC), renowned for its exceptional electrical resistivity, remarkable thermal conductivity, and chemical inertness, has been successfully employed as a support matrix for Ru-catalyzed ammonia decomposition, facilitating intensified reactant-catalyst interactions through its intricate pore architecture and superior heat dissipation properties, as depicted in Fig. 9a-c.<sup>80</sup> In addition, the related derivatives, MWCNTs, also exhibit excellent catalytic activity, and their special electronic properties facilitate the transfer of electrons from the active sites on the carriers.<sup>81</sup> This suggests that the modulation of the Ru active centers by different carriers through strong metal-support interactions can promote the ammonia decomposition reaction at the surface of the catalysts.

Table 2 summarizes the typical loaded catalysts for ammonia decomposition. Recent studies have underscored the ability of the  $\text{Mg}_{1-x}\text{Ni}_x\text{O}$  solid solution to facilitate Ni migration to the surface upon high-temperature hydrogen activation, yielding Ni/MgO catalysts with enhanced Ni particle dispersion. Notably, the attainment of higher Ni dispersion and loading within these catalysts significantly boosts their catalytic activity for ammonia decomposition reactions. This correlation between structural features and



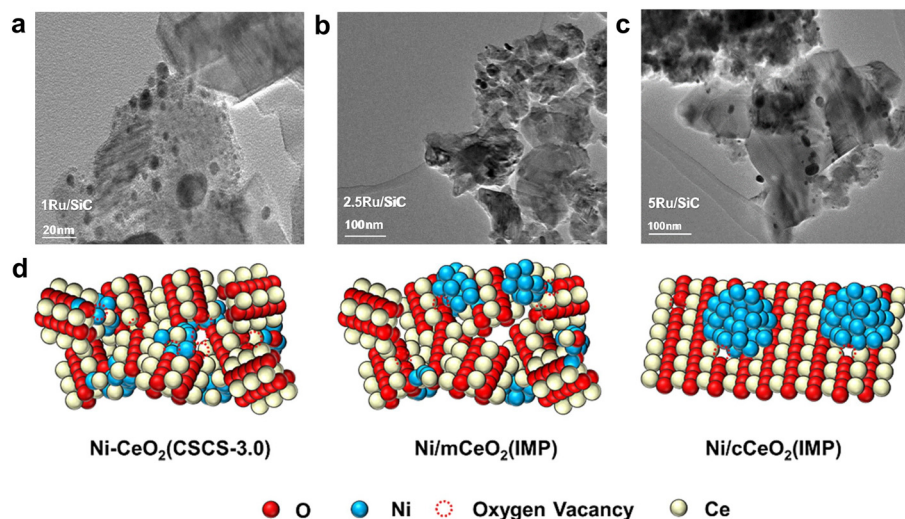


**Fig. 9** Ru catalysts supported by SiC. (a) 2.5 Ru/SiC, (b) 2.5Ru/SiC and (c) 5Ru/SiC reduced at 673 K are shown in TEM pictures.<sup>80</sup> Re-drawing from ref. 80. Copyright 2021, Elsevier. (d) Modelling of the structures of Ni-CeO<sub>2</sub>(CSCS-3.0), Ni/mCeO<sub>2</sub>(IMP), and Ni/cCeO<sub>2</sub>(IMP).<sup>82</sup> Copyright 2023, Elsevier.

**Table 2** Summary of previously reported typical loaded catalysts and their applications in ammonia decomposition reactions

| Active phase | Wt (%) | Support                        | WHSV (mL g <sup>-1</sup> h <sup>-1</sup> ) | GHSV (h <sup>-1</sup> ) | NH <sub>3</sub> inlet flow (%) | T (°C) | Conv (%) | E <sub>a</sub> (kJ mol <sup>-1</sup> ) | TOF (s <sup>-1</sup> ) | Ref. |
|--------------|--------|--------------------------------|--|-------------------------|--------------------------------|--------|----------|--|------------------------|------|
| Ru           | 4.8    | TiO <sub>2</sub>               | 30 000                                     |                         | 100                            | 450    |          | 61                                     | 3.1                    | 90   |
| Ru           | 2      | ZrO <sub>2</sub>               | 240 000                                    | 80 000                  | 50                             | 500    | 98       |  |                        | 91   |
| Ru           | 1.9    | Al <sub>2</sub> O <sub>3</sub> | 30 000                                     |                         | 100                            | 500    | 85       | 80                                     |                        | 92   |
| Ru           | 3.5    | MgO                            | 36 000                                     |                         | 100                            | 450    | 87       | 58                                     |                        | 93   |
| Ru           | 25     | C                              | 30 000                                     |                         | 100                            | 400    | 42       | 54                                     |                        | 94   |
| Ru           | 5      | AC                             | 30 000                                     |                         | 100                            | 450    | 40       |  |                        | 95   |
| Ru           | 5      | CNTs                           | 30 000                                     |                         | 100                            | 500    | 88       | 69                                     |                        | 96   |
| Ru           | 4.7    | MWCNT                          | 9000                                       |                         | 100                            | 400    | 31       |  |                        | 97   |
| Ru           | 0.8    | N-CNTs                         | 42 000                                     |                         | 100                            | 550    | 61       |  | 18.8                   | 98   |
| Ni           | 30     | CeO <sub>2</sub>               |  | 12 000                  | 100                            | 500    | 60       |  | 0.7                    | 99   |
| Ni           | 6      | MgO                            |  | 1800                    | 100                            | 650    | 88       |  |                        | 100  |
| Fe           | 28     | MgO                            | 120 000                                    |                         | 3                              | 450    | 24       | 70                                     |                        | 101  |
| Fe           | 5      | CNTs                           | 6000                                       |                         | 100                            | 500    | 15       | 142                                    |                        | 102  |
| Co           | 5      | Al <sub>2</sub> O <sub>3</sub> | 36 000                                     |                         | 100                            | 500    | 21       |  |                        | 103  |
| Co           | 5      | CNTs                           | 6000                                       |                         | 100                            | 500    | 61       | 93                                     |                        | 102  |

catalytic performance is meticulously examined through complementary *in situ* characterization techniques, which also provide insights into the intricate metal-support interactions.<sup>83</sup> In addition to MgO, various metal oxide materials such as SiO<sub>2</sub>, La<sub>2</sub>O<sub>3</sub>, CeO<sub>2</sub>, Y<sub>2</sub>O<sub>3</sub>, Al<sub>2</sub>O<sub>3</sub>, *etc.*<sup>84–86</sup> are also often applied as carriers for the preparation of nickel-based catalysts, and among these oxide carriers, CeO<sub>2</sub>, due to the advantages of large oxygen storage and abundant surface defect, exhibits modifiable metal-supported interaction.<sup>87</sup> Constructing different nanostructures might enhance the metal-support interactions between Ni and CeO<sub>2</sub>. Jiang *et al.* designed CeO<sub>2</sub> morphologies including rods (R), spheres, and spindles and found that the Ni/CeO<sub>2</sub>-R catalyst exhibited the best performance, which could be attributed to the formation of the smaller Ni particles (3.3 nm) on the rod-like CeO<sub>2</sub> support.<sup>88</sup> The influence of CeO<sub>2</sub> supports fabricated *via* distinct preparation methodologies exhibits different metal-support interactions within Ni/CeO<sub>2</sub> systems. Notably,

Ni-CeO<sub>2</sub> nanocomposites synthesized through the innovative approach, incorporating silica sol templates during colloidal solution combustion in the synthesis process, feature uniformly dispersed, small-sized Ni nanoparticles embedded within the CeO<sub>2</sub> nanoparticle matrix. This unique configuration fosters enhanced interactions and enriched Ni-CeO<sub>2</sub> interface, enabling the modulation of metal-support interactions for further augmentation of catalytic activity (Fig. 9d).<sup>82</sup> Furthermore, the primary metal-support interactions for the Ni-based catalysts supported on carbonaceous materials share similarities with that observed in Ru-based catalysts. Both systems harness the high specific surface area to elevate metal particle dispersion and leverage the exceptional electrical conductivity of carbon materials to expedite electron transport at the catalyst surface, thereby contributing to enhanced catalytic performance.<sup>89</sup> Similarly, Fe-based and Co-based catalysts are also included. Strong metal-support interactions are the most used design





approach in existing ammonia decomposition catalysts. The existing literature reports show that the activities of transition metals combined with different carriers have been improved to a certain extent, but there is still a gap compared with the optimal Ru-based catalysts, so further optimization of the catalyst design is needed.

#### 4.4 Alloying effect

While Ru has garnered recognition as the most potent catalyst, its prohibitively high cost has posed significant barriers to widespread industrial adoption. Consequently, countless researchers have begun extensive studies of various non-precious metal alternatives.<sup>104,105</sup> In the search for innovative active centers capable of matching the performance of Ru nanoparticles, a number of studies have emphasized the critical importance of alloying effects in the development of novel highly active catalytic sites. These findings highlight the potential for alloy-based catalysts to offer cost-effective solutions while maintaining or even surpassing the catalytic performance of their noble metal counterparts.<sup>106</sup> Alloy catalysts for ammonia decomposition consist of two main categories: poly (binary/ternary) alloys and high-entropy alloys (HEAs).

**4.4.1 Poly alloys.** Compared to existing monometallic catalysts, such as Fe,<sup>107,108</sup> Ni,<sup>97</sup> and Co<sup>109</sup> ammonia decomposition catalysts, alloyed catalysts that consist of two or more metals have the advantage of higher catalytic activity, which is mainly reflected in the alloying effect.<sup>110</sup> Periodic table interpolation theory suggests that the N-binding energies of the alloys are linear combinations of the parent metals.<sup>111</sup> Therefore, by alloying a variety of metals with different N-binding energies, optimized intermediate binding energies can be formed (resulting in Ru-like intermediate metal–N-binding energies), which can contribute to the improvement of ammonia decomposition catalytic capability.

Bimetallic alloy catalysts have been widely studied in the field of ammonia decomposition, including Fe–Ni,<sup>112</sup> Fe–Co,<sup>113</sup> Co–Mo,<sup>114</sup> and Co–Re.<sup>115</sup> With the continuous development of bimetallic alloy catalysts, the combination of DFT calculations and scanning tunneling microscopy studies has shown that surface microstructures, defects, or detached metal atoms may have a significant impact on the reaction.<sup>116</sup> For the nickel-related alloy catalysts, the N\*–N\* (two neighboring surface N atoms) conjugation process is more favorable for the reaction in the uncoordinated ladder/edge sites than in the step sites.<sup>117</sup> Therefore, this effect was taken into account in the design of Pt–Ni bimetallic catalysts by constructing rational core–shell nanoparticle models, the

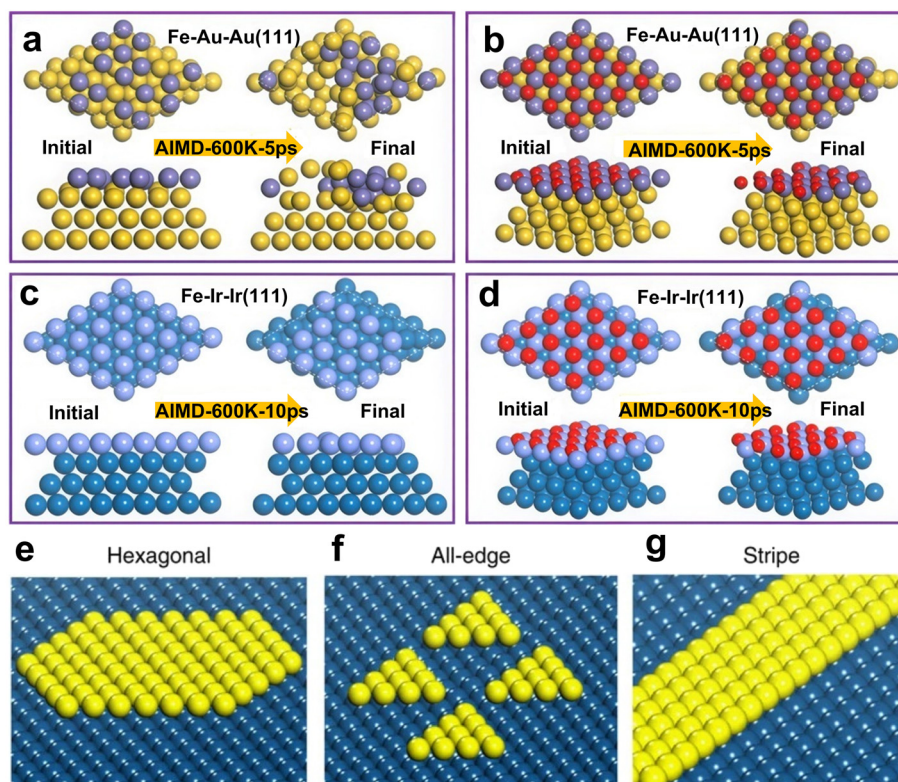


**Fig. 10** The bimetallic surface simulated by AIMD at 600 K, a high temperature. (a) Fe–Au–Au(111) devoid of N\*; (b) Fe–Au–Au(111) supplemented with 1 mL N\*; (c) Fe–Ir–Ir(111) devoid of N\*; (d) Fe–Ir–Ir(111) augmented with 1 mL N\*. Observe the atomic structures from all angles in the insets in (a)–(d). The atoms of N are shown by the red spheres.<sup>119</sup> Re-drawing from ref. 119. Copyright 2021, American Chemical Society. (e–g) Diagrams of Ni patches on Pt (111) showing the (110) and (100) stages, with forms ranging from hexagonal to all-edge and stripe Ni clusters. The ratio of terrace and step sites changes in (e) or stays constant in (f) and (g) when the Ni loading is changed.<sup>118</sup> Copyright 2015, Nature Publishing Group.



ideal bimetallic surface (Ni–Pt–Pt), and the patched bimetallic surface on Pt with different Ni loadings (as shown in Fig. 10e–g). To gain insight into the structural sensitivity and active sites, Guo *et al.* showed through multiscale steady-state simulations that dual sites formed around adequately small guest metal clusters, hence augmenting catalytic activity.<sup>118</sup> Inspired by this, Wu *et al.* screened a variety of transition metal–precious metal alloy catalysts for NH<sub>3</sub> decomposition. The NH<sub>3</sub> decomposition volcano diagrams showed that Ni–Au–Au(111), Fe/Ni–Ag–Ag(111), Fe–Ir–Ir(111), Fe/Ni–Pd–Pd(111), and Fe/Co/Ni–Pt–Pt(111) were the micro-interfacial catalysts with better structural modulation of N\*–covered surfaces. The *ab initio* molecular dynamics (AIMD) simulated structural evolutions of Fe–Au–Au(111) and Fe–Ir–Ir(111) surfaces were selected as examples for illustration, as shown in Fig. 10a–d. The AIMD simulated structural evolutions indicate that bonding interactions between N\* and guest atoms are favorable for regulating the stability of bimetallic sheets of different configurations.<sup>119</sup> These studies provide guidance for the modulation of various polymetallic surfaces in the field of NH<sub>3</sub> decomposition.

**4.4.2 High-entropy alloys.** Although bimetallic alloy catalysts have been widely used in ammonia decomposition, they are still limited by a large immiscible gap, which restricts the continuous adjustment of component ratios.<sup>120</sup> In contrast, HEAs break the immiscible gap among elements, facilitate robust control of elemental concentrations, and promote optimization of catalytic properties.<sup>121</sup> Therefore, some researchers have used HEAs as ammonia decomposition catalysts. The HEA CoMoFeNiCu nanoparticles could robustly regulate the Co/Mo ratio, break the miscibility limitation of the traditional bimetallic Co–Mo catalysts, and the catalytic activity over the novel catalyst was even more than 20 times that over the single Ru catalyst. Fig. 11a shows the NH<sub>3</sub> degradation on the HEA CoMoFeNiCu running continuously at 500 °C for 50 h; the catalytic activity basically remains unchanged. The catalysts after such a long durability test are characterized by elemental mapping (see inset in Fig. 11a), with almost no change in the alloy homogeneity or surface composition, which confirms the durability and stability. Based on Sabatier's principle, the more cobalt-rich catalyst binds too

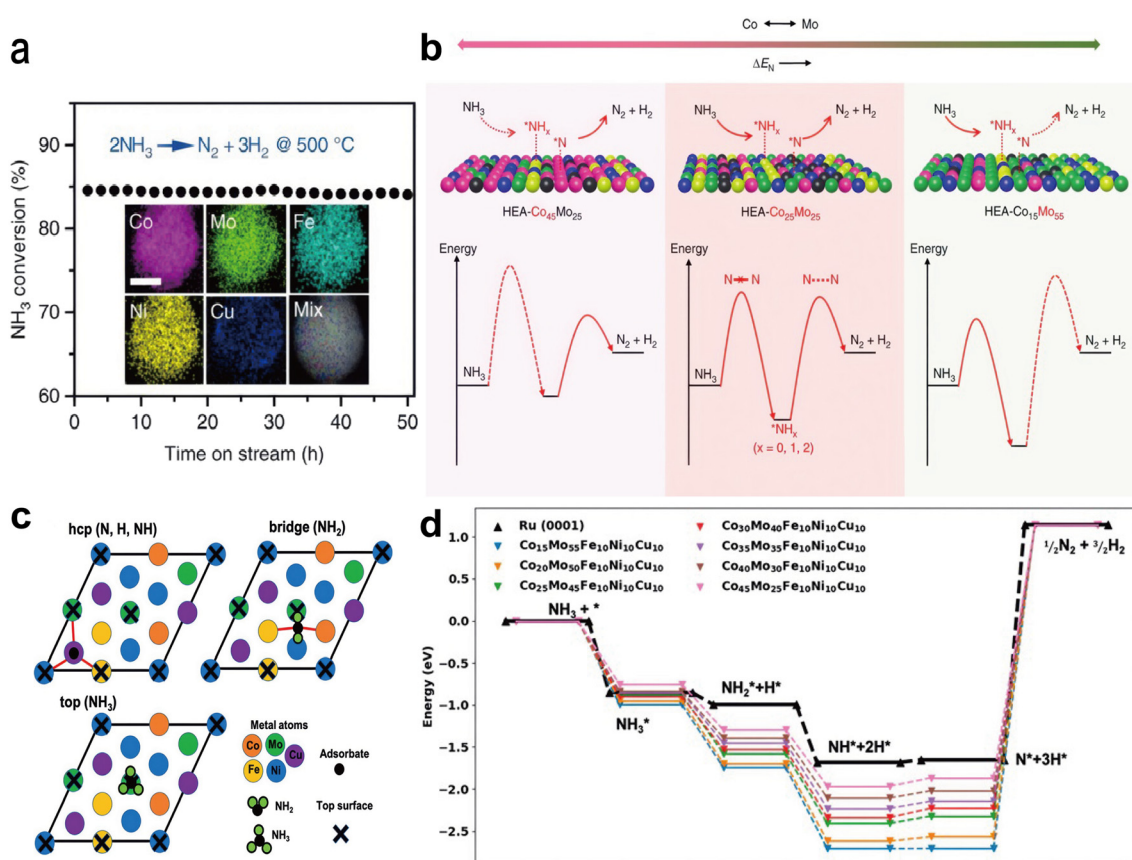


**Fig. 11** (a) Evaluation of the HEA–Co<sub>25</sub>Mo<sub>45</sub> catalyst's stability at 500 °C. Featured image: catalyst element map after stability test; scale bar = 10 nm. (b) Visual representation of the parameters that restrict the rate of NH<sub>3</sub> decomposition. A balance between the two processes is achieved on an intermediate composition (HEA–Co<sub>25</sub>Mo<sub>45</sub>) when the rate is restricted by the activation or dehydrogenation of NH<sub>3</sub> on a Co-rich surface (left) and by the recombinative desorption of \*N on a Mo-rich surface.<sup>122</sup> Copyright 2019, Nature Publishing Group. (c) An overview of the adsorption configurations for several chemical species on a typical HEA fcc (111) surface. (d) The energy landscape of ammonia decomposition for Co<sub>x</sub>Mo<sub>y</sub>–Fe<sub>10</sub>Ni<sub>10</sub>Cu<sub>10</sub> related to varying amounts of Co and Mo. To facilitate comparison, the relevant Ru(0001) values are shown. On the slab, an empty adsorption site is shown by an asterisk (\*), whereas a site filled by species A is indicated by A\*.<sup>123</sup> Copyright 2021, American Chemical Society.



weakly to N and thus produces a rather high kinetic barrier to dehydrogenation ( $\text{NH}_3 \rightarrow \text{*NH}_2 \rightarrow \text{*NH} \rightarrow \text{*N}$ ), while the more molybdenum-rich binds too strongly to N and gives recombined species desorbed from the surface ( $2\text{*N} \rightarrow \text{N}_2$ ), and the tradeoff between these two factors produces the optimal intermediate binding energy for the reaction (Fig. 11b). This finding can be further correlated with the dependence of  $\Delta E_N$  on the number of reaction stages. In addition, this study proposes that the catalytic activity and kinetics of the HEA catalysts mainly depend on the hybrid surface site mechanism, which also corresponds to the aforementioned micro-surface structure modulation of the bimetallic catalysts. By rationally adjusting the composition and geometry of HEAs, it is possible to obtain high-entropy alloy-based catalysts with higher modulation activity.<sup>122</sup> Hence, on the basis of the above study, Saidi *et al.* performed high-throughput DFT calculations of nitrogen adsorption of various components on the surface of CoMoFeNiCu HEA(111) and found that the strongest nitrogen adsorption was observed at the hexagonal close-packed (hcp) sites (Fig. 11c). Computational modeling and machine learning were applied

to further optimize the ratios of metal elements in the CoMoFeNiCu HEA catalysts. By comparing the full energy paths of the HEA and Ru(0001) with different ratios in the dehydrogenation step of  $\text{NH}_3$  (Fig. 11d), it was found that the HEA binds the intermediates more strongly than Ru, and the stability of  $\text{NH}_2$  intermediates was significantly higher than that over Ru(0001) in the optimal doping range.<sup>123</sup> The above study provides new ideas for the development and optimization of other HEA catalysts and expands the application of the alloying effect in ammonia decomposition reactions.

The above four commonly used methods are the key considerations in the design of ammonia decomposition catalysts. There are complementarities and constraints among the methods, which require careful consideration of the equilibrium among the elements of the whole catalyst system, the three-dimensional structural distribution, and the structural modulation of the reaction micro interfaces in order to achieve a good balance of  $\text{NH}_3$  adsorption and N/H shedding on the surface active sites and then to promote the ammonia decomposition reaction.

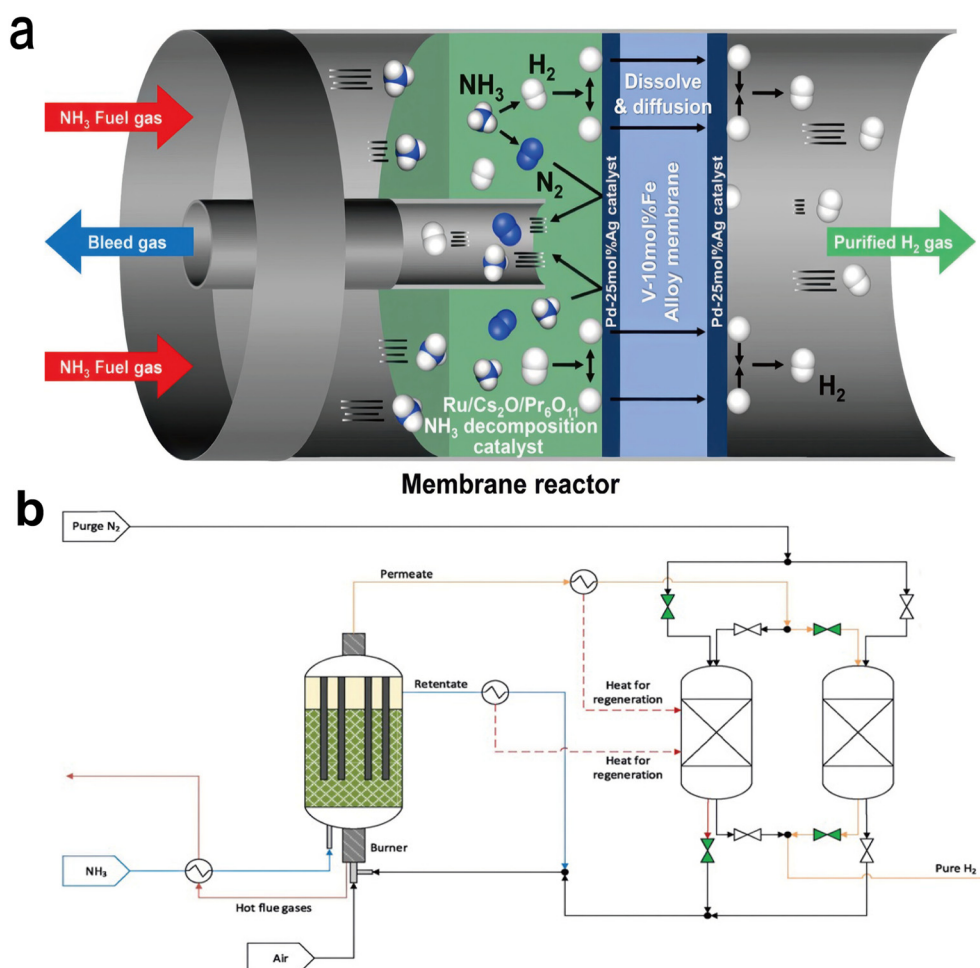


Fig. 12 (a) The membrane reactor for separating and purifying hydrogen from  $\text{NH}_3$  gas is shown schematically.<sup>124</sup> Copyright 2022, Elsevier. (b) The ammonia-based hydrogen generation system is put up for experimental purposes.<sup>131</sup> Copyright 2022, Elsevier.





## 5 Catalysts for different ammonia decomposition reactors

The application of  $\text{NH}_3$  decomposition for the production of hydrogen energy fuels generally requires two steps, namely the decomposition of ammonia to produce hydrogen and nitrogen and the separation and purification of hydrogen.<sup>124</sup> Of these, catalysts for  $\text{NH}_3$  decomposition, not limited to the catalysts mentioned above, are under development. In order to facilitate the second  $\text{H}_2$  separation and purification step, the design of catalysts also needs to be integrated with industrial reactors.<sup>125–127</sup> For example, V–Fe alloy membranes and  $\text{Ru}/\text{Cs}_2\text{O}/\text{Pr}_6\text{O}_{11}$  catalysts were employed in the membrane reactors (Fig. 12a).<sup>124</sup> Carbon nanofiber-loaded Fe, Mo, and Co catalysts were applied in microwave reactors.<sup>128,129</sup>  $\text{MgAl}_2\text{O}_4$  catalysts were used as ammonia decomposition catalysts under plasma-excited reaction conditions to produce hydrogen.<sup>130</sup> However, the composition and structure of ammonia decomposition catalysts still need to be further integrated with the reactor in order to ensure the high performance of the catalysts in real applications.

The present reactors applied to on-site  $\text{H}_2$  production from  $\text{NH}_3$  decomposition are dominated by membrane reactors, which are considered to be the most efficient from the point of energy consumption and operating costs.<sup>132</sup> The membrane reactors are very compact because the ammonia decomposition and hydrogen separation are integrated into a single reactor, while the catalysts and membranes might interact in the same reaction field.<sup>124</sup> Consequently, improving the decomposition rate of  $\text{NH}_3$  could be achieved by membrane separation of  $\text{H}_2$  during the  $\text{NH}_3$  decomposition process. Cechetto *et al.* used a double-layer Pd–Ag membrane, 2 wt%  $\text{Ru}/\text{Al}_2\text{O}_3$  catalyst, and 13X molecular sieves in a membrane reactor to improve the hydrogen purity and production efficiency by adjusting the thickness of the alloy membranes (more than 6  $\mu\text{m}$ ) (Fig. 12b).<sup>131</sup> In recent years, the application of plasma and microwave in catalytic reactions has received great attention.<sup>133,134</sup> The hydrogen production rate in the plasma reactor mainly depends on the plasma type, catalyst type, discharge frequency, and  $\text{NH}_3$  flow rate (Table 3).<sup>134</sup> The main plasma types include dielectric barrier discharge (DBD), alternating current (AC) arc, and gliding arc discharge (GAD). Hayakawa *et al.* designed a new plasma membrane reactor (PMR) with a  $\text{Pd}_{0.60}\text{--Cu}_{0.40}$  alloy film as the  $\text{H}_2$  separation membrane, 10

wt%  $\text{Ni}/\text{Al}_2\text{O}_3$  as the catalyst, and plasma excitation as the supply energy for the separation of high-purity  $\text{H}_2$  from  $\text{NH}_3$  decomposition gases.<sup>135</sup> For  $\text{NH}_3$  decomposition microwave reactors, the key point for better energy absorption and transfer is to load the catalyst bed on the materials (*e.g.*, carbon) with high microwave-absorbing properties.<sup>18,129</sup> Yildiz *et al.* used a 1:1 physical mixture of  $\text{Mo}/\text{Al}_2\text{O}_3$  catalyst and mesoporous carbon in a microwave reactor, achieving a 98% ammonia decomposition rate at 350 °C.<sup>136</sup> Although a range of catalysts has been incorporated into the reactor, the ongoing development of catalysts tailored for various application scenarios remains crucial to facilitate the widespread adoption of  $\text{NH}_3$  decomposition for hydrogen production.

## 6 Summary and perspective

Hydrogen production by ammonia decomposition is an efficient, convenient, green, and low-carbon method that has attracted much attention. However, the depth and breadth of the existing studies are far from the practical needs of application to hydrogen production. In this review, by summarizing the existing literature to illustrate the main difficulties in the continuous advancement of the ammonia decomposition reaction. Focusing on the urgent challenge of designing and developing efficient ammonia decomposition catalysts, we summarize the four major design strategies of catalysts, *i.e.*, the size effect, alkalinity modulation, metal–support interactions, and alloying effect. Based on these, the catalysts involved in existing ammonia decomposition reactors were divided. Literature analysis shows that despite significant progress in the study of ammonia decomposition catalysts, great efforts are still needed in the aspects related to the design of ammonia decomposition catalysts. There are still many challenges in the field of ammonia decomposition that need to be addressed, such as the following. (1) Due to the special nature of the ammonia decomposition reaction, which is sensitive to the micro-reaction environment and external conditions such as temperature and pressure, the existing kinetic and theoretical calculations cannot accurately describe the specific course of the catalyst micro-reaction interface under the actual reaction conditions, and it is still necessary to explore a more scientific and perfect theoretical calculation model. (2) The studies on the reaction mechanisms of ammonia decomposition on different catalyst surfaces are not perfect enough, and the interaction

**Table 3** Summary of previously reported catalysts and their applications in ammonia decomposition plasma reactors

| Plasma        | Reactor                                       | Catalyst                          | Catalyst support        | $\text{NH}_3$ conversion (%) | $\text{H}_2$ production                | Ref. |
|---------------|---|-----------------------------------|-------------------------|------------------------------|--|------|
| DBD           | Plasma-catalytic plate reactor                | $\text{Al}_2\text{O}_3$           |                         | 83                           |  | 137  |
|               | Plasma-catalytic plate microreactor           | $\text{Ru}$ and $\text{SiO}_2$    | $\text{Al}_2\text{O}_3$ | 85                           |  | 138  |
|               | DBD plasma-catalytic reactor                  | Fe-based catalyst                 |                         | 99                           | 80 mol $\text{L}^{-1}$ $\text{h}^{-1}$ | 139  |
|               | Catalytic decomposition reactor (CDR) and PMR | $\text{Ni}/\text{Al}_2\text{O}_3$ |                         | 99                           | 120 L $\text{h}^{-1}$                  | 135  |
| AC arc plasma | AC arc discharge reactor                      | SS, Ni, and Cu electrodes         |                         | >99%                         |  | 140  |
| Arc plasma    | Nonthermal arc reactor                        | NiO                               | $\text{Al}_2\text{O}_3$ |                              | ~35%                                   | 141  |



conditions corresponding to various mechanisms and the constitutive relationship of catalytic materials are not clear yet. (3) All four catalyst design strategies need to be considered in a balanced manner, but the correlation and constraints among the strategies have not been clarified, which is an obvious obstacle to the design and development of catalysts. (4) Currently, most of the studies have explored only the performance of catalysts under conventional thermal field conditions, and few studies have been conducted on the combination of different reaction conditions and reactor configurations involved in actual on-site hydrogen production applications, which is not conducive to the application of ammonia decomposition catalysts. (5) There are few *in situ* characterization means for real-time measurement of the catalyst during the reaction process. Due to the wide temperature window of the ammonia decomposition reactor during practical application, it is difficult to confirm the changes of the catalyst during the reaction process, which is also an important difficulty hindering its practical application. For these reasons, the employment of DFT, numerical modeling and machine learning simulations holds significant potential in expediting the research endeavor by verifying the underlying mechanisms of ammonia decomposition. This approach not only simulates ammonia decomposition reactions across diverse reaction conditions but also reinforces experimental design strategies, thereby facilitating the experimental validation of theoretical hypotheses. Furthermore, the integration of advanced *in situ* characterization and testing methodologies into the experimental protocol of ammonia decomposition underscores a bidirectional momentum, propelling continuous advancements in this technology both theoretically and practically.

## Data availability

Data are available on request from the authors.

## Conflicts of interest

The authors declare no conflict of interest.

## Acknowledgements

This work was supported by the Natural Science Foundation of China (22476004, 21961160743, and 21622701), the Key Science and Technology Projects of Beijing Municipal Education Commission (KZ202210005011), and the Natural Science Foundation of Hebei (B2021208033).

## References

- 1 C. H. Christensen, T. Johannessen, R. Z. Sørensen and J. K. Nørskov, Towards an ammonia-mediated hydrogen economy?, *Catal. Today*, 2006, **111**, 140–144.
- 2 E. J. Cairns, E. L. Simons and A. D. Tevebaugh, Ammonia-oxygen fuel cell, *Nature*, 1968, **217**, 780–781.
- 3 D. S. Dhawale, S. Biswas, G. Kaur and S. Giddey, Challenges and advancement in direct ammonia solid oxide fuel cells: A review, *Inorg. Chem. Front.*, 2023, **10**, 6176–6192.
- 4 F. Dawood, M. Anda and G. M. Shafiullah, Hydrogen production for energy: An overview, *Int. J. Hydrogen Energy*, 2020, **45**, 3847–3869.
- 5 T. Wu, B. Chang, Y. Li, X. Zhang, X. Zhao, Z. Liu, G. Zhang, X. Liu, L. Zhao, Y. Zhang, H. Zhang, H. Liu and W. Zhou, Laser-induced plasma and local temperature field for high-efficiency ammonia synthesis, *Nano Energy*, 2023, **116**, 108855.
- 6 S. Chen, S. Perathoner, C. Ampelli, C. Mebrahtu, D. Su and G. Centi, Electrocatalytic synthesis of ammonia at room temperature and atmospheric pressure from water and nitrogen on a carbon-nanotube-based electrocatalyst, *Angew. Chem., Int. Ed.*, 2017, **56**, 2699–2703.
- 7 R. Paul, N. Maity, B. Das, S. S. Emadian, A. Kumar, S. Krishnamurthy, A. K. Singh and R. Ghosh, Efficient detection of 45 ppb ammonia at room temperature using Ni-doped CeO<sub>2</sub> octahedral nanostructures, *J. Colloid Interface Sci.*, 2024, **662**, 663–675.
- 8 S. Mukherjee, S. V. Devaguptapu, A. Sviripa, C. R. F. Lund and G. Wu, Low-temperature ammonia decomposition catalysts for hydrogen generation, *Appl. Catal., B*, 2018, **226**, 162–181.
- 9 K. Honkala, A. Hellman, I. N. Remediakis, A. Logadottir, A. Carlsson, S. Dahl, C. H. Christensen and J. K. Nørskov, Ammonia synthesis from first-principles calculations, *Science*, 2005, **307**, 555–558.
- 10 S. Kang, J. Cha, Y. S. Jo, Y. Lee, H. Sohn, Y. Kim, C. K. Song, Y. Kim, D. Lim, J. Park and C. W. Yoon, Heteroepitaxial growth of B<sub>5</sub>-site-rich Ru nanoparticles guided by hexagonal boron nitride for low-temperature ammonia dehydrogenation, *Adv. Mater.*, 2022, **35**, 2203364.
- 11 S. Dahl, E. Törnqvist and I. Chorkendorff, Dissociative adsorption of N<sub>2</sub> on Ru(0001): A surface reaction totally dominated by steps, *J. Catal.*, 2000, **192**, 381–390.
- 12 S. Ristig, M. Poschmann, J. Folke, O. Gómez-Cápiro, Z. Chen, N. Sanchez-Bastardo, R. Schlögl, S. Heumann and H. Ruland, ammonia decomposition in the process chain for a renewable hydrogen supply, *Chem. Ing. Tech.*, 2022, **94**, 1413–1425.
- 13 S. Gong, Z. Du, Y. Hu and W. Yao, Role of cation in catalytic decomposition of ammonia over Ni supported zeolite Y catalysts, *Int. J. Hydrogen Energy*, 2024, **63**, 547–555.
- 14 X. Han, M. Hu, J. Yu, X. Xu, P. Jing, B. Liu, R. Gao and J. Zhang, Dual confinement of LaCoO<sub>x</sub> modified Co nanoparticles for superior and stable ammonia decomposition, *Appl. Catal., B*, 2023, **328**, 122534.
- 15 B. Teng, C. Ma, J. Chen, Y. Zhang, B. Wei, M. Sang, H. Wang and Y. Sun, Ru dispersed on oxygen-defect-rich CeO<sub>2</sub> nanorods for ammonia decomposition, *ACS Appl. Nano Mater.*, 2024, **7**, 15012–15024.
- 16 H. Fang, S. Wu, T. Ayvali, J. Zheng, J. Fellowes, P. L. Ho, K. C. Leung, A. Large, G. Held, R. Kato, K. Suenaga, Y. I. A. Reyes, H. V. Thang, H. Y. T. Chen and S. C. E. Tsang,



- Dispersed surface Ru ensembles on MgO(111) for catalytic ammonia decomposition, *Nat. Commun.*, 2023, **14**, 647.
- 17 J. Li, B. Sheng, Y. Chen, J. Yang, P. Wang, Y. Li, T. Yu, H. Pan, L. Qiu, Y. Li, J. Song, L. Zhu, X. Wang, Z. Huang and B. Zhou, Utilizing full-spectrum sunlight for ammonia decomposition to hydrogen over GaN nanowires-supported Ru nanoparticles on silicon, *Nat. Commun.*, 2024, **15**, 7393.
  - 18 D. Varisli, C. Korkusuz and T. Dogu, Microwave-assisted ammonia decomposition reaction over iron incorporated mesoporous carbon catalysts, *Appl. Catal., B*, 2017, **201**, 370–380.
  - 19 R. C. Seyfeli and D. Varisli, Performance of microwave reactor system in decomposition of ammonia using nickel based catalysts with different supports, *Int. J. Hydrogen Energy*, 2022, **47**, 15175–15188.
  - 20 D. Yuan, F. Xie, K. Li, Q. Guan, J. Hou, S. Yang, G. Han, X. San, J. Hao and Y. Li, Atomic strategy to boost the solar heating ammonia decomposition of cobalt-based catalyst, *Appl. Surf. Sci.*, 2023, **613**, 155973.
  - 21 L. Zhang, Y. Cong, W. Yang and L. Lin, A Direct ammonia tubular solid oxide fuel cell, *Chin. J. Catal.*, 2007, **28**, 749–751.
  - 22 K. Zheng, Y. Yan, Y. Sun, J. Yang, M. Zhu, M. Ni and L. Li, An experimental study of ammonia decomposition rates over cheap metal catalysts for solid oxide fuel cell anode, *Int. J. Hydrogen Energy*, 2023, **48**, 19188–19195.
  - 23 D. K. Lim, A. B. Plymill, H. Paik, X. Qian, S. Zecevic, C. R. I. Chisholm and S. M. Haile, Solid acid electrochemical cell for the production of hydrogen from ammonia, *Joule*, 2020, **4**, 2338–2347.
  - 24 J. Łuczak and M. Lieder, Nickel-based catalysts for electrolytic decomposition of ammonia towards hydrogen production, *Adv. Colloid Interface Sci.*, 2023, **319**, 102963.
  - 25 J. Džibelová, S. M. H. Hejazi, V. Šedajová, D. Panáček, P. Jakubec, Z. Baďura, O. Malina, J. Kašlík, J. Filip, Š. Kment, M. Otyepka and R. Zbořil, Hematene: A sustainable 2D conductive platform for visible-light-driven photocatalytic ammonia decomposition, *Appl. Mater. Today*, 2023, **34**, 101881.
  - 26 S. Armenise, F. Cazaña, A. Monzón and E. García-Bordejé, In situ generation of CO<sub>x</sub>-free H<sub>2</sub> by catalytic ammonia decomposition over Ru-Al-monoliths, *Fuel*, 2018, **233**, 851–859.
  - 27 P. Yu, J. Guo, L. Liu, P. Wang, G. Wu, F. Chang and P. Chen, Ammonia decomposition with manganese nitride–calcium imide composites as efficient catalysts, *ChemSusChem*, 2016, **9**, 364–369.
  - 28 G. Djéga-Mariadassou, C. H. Shin and G. Bugli, Tamaru's model for ammonia decomposition over titanium oxynitride, *J. Mol. Catal. A: Chem.*, 1999, **141**, 263–267.
  - 29 C. Egawa, T. Nishida, S. Naito and K. Tamaru, Ammonia decomposition on (11 10) and (001) surfaces of ruthenium, *J. Chem. Soc., Faraday Trans. 1*, 1984, **80**, 1595.
  - 30 V. L. Kuchaeu, E. N. Shapatina and A. K. Avetisov, Mechanism of oxygen poisoning of ammonia synthesis catalyst, *Russ. J. Electrochem.*, 2009, **45**, 983–995.
  - 31 H. He, H. Jiang, F. Yang, J. Liu, W. Zhang, M. Jin and Z. Li, Bimetallic Ni<sub>x</sub>Co<sub>10-x</sub>/CeO<sub>2</sub> as highly active catalysts to enhance mid-temperature ammonia decomposition: Kinetics and synergies, *Int. J. Hydrogen Energy*, 2023, **48**, 5030–5041.
  - 32 I. Lucentini, G. García Colli, C. D. Luzi, I. Serrano, O. M. Martínez and J. Llorca, Catalytic ammonia decomposition over Ni-Ru supported on CeO<sub>2</sub> for hydrogen production: Effect of metal loading and kinetic analysis, *Appl. Catal., B*, 2021, **286**, 119896.
  - 33 S. T. Oyama, Kinetics of ammonia decomposition on vanadium nitride, *J. Catal.*, 1992, **133**, 358–369.
  - 34 A. K. Hill and L. Torrente-Murciano, Low temperature H<sub>2</sub> production from ammonia using ruthenium-based catalysts: Synergetic effect of promoter and support, *Appl. Catal., B*, 2015, **172–173**, 129–135.
  - 35 Y. Wang, M. R. Kunz, S. Siebers, H. Rollins, J. Gleaves, G. Yablonsky and R. Fushimi, Transient kinetic experiments within the high conversion domain: The case of ammonia decomposition, *Catalysts*, 2019, **9**, 104.
  - 36 D. A. Hansgen, D. G. Vlachos and J. G. Chen, Using first principles to predict bimetallic catalysts for the ammonia decomposition reaction, *Nat. Chem.*, 2010, **2**, 484–489.
  - 37 A. Logadottir, T. H. Rod, J. K. Nørskov, B. Hammer, S. Dahl and C. J. H. Jacobsen, The Brønsted–Evans–Polanyi relation and the volcano plot for ammonia synthesis over transition metal catalysts, *J. Catal.*, 2001, **197**, 229–231.
  - 38 A. Boisen, S. Dahl, J. K. Nørskov and C. H. Christensen, Why the optimal ammonia synthesis catalyst is not the optimal ammonia decomposition catalyst, *J. Catal.*, 2005, **230**, 309–312.
  - 39 J. K. Nørskov, T. Bligaard, A. Logadottir, S. Bahn, L. B. Hansen, M. Bollinger, H. Bengaard, B. Hammer, Z. Sljivancanin, M. Mavrikakis, Y. Xu, S. Dahl and C. J. H. Jacobsen, Universality in heterogeneous catalysis, *J. Catal.*, 2002, **209**, 275–278.
  - 40 C. J. H. Jacobsen, S. Dahl, A. Boisen, B. S. Clausen, H. Topsøe, A. Logadottir and J. K. Nørskov, Optimal catalyst curves: Connecting density functional theory calculations with industrial reactor design and catalyst selection, *J. Catal.*, 2002, **205**, 382–387.
  - 41 N. Turaeva, R. Fushimi and G. Yablonsky, Kinetic expression for optimal catalyst electronic configuration: The case of ammonia decomposition, *J. Phys. Chem. C*, 2020, **124**, 26310–26319.
  - 42 J. C. Ganley, F. S. Thomas, E. G. Seebauer and R. I. Masel, A priori catalytic activity correlations: The difficult case of hydrogen production from ammonia, *Catal. Lett.*, 2004, **96**, 117–122.
  - 43 L. Wang, Y. Zhao, C. Liu, W. Gong and H. Guo, Plasma driven ammonia decomposition on a Fe-catalyst: Eliminating surface nitrogen poisoning, *Chem. Commun.*, 2013, **49**, 3787.
  - 44 T. E. Bell and L. Torrente-Murciano, H<sub>2</sub> production via ammonia decomposition using non-noble metal catalysts: A review, *Top. Catal.*, 2016, **59**, 1438–1457.





- 45 C. J. H. Jacobsen, S. Dahl, B. S. Clausen, S. Bahn, A. Logadottir and J. K. Nørskov, Catalyst design by interpolation in the periodic table: Bimetallic ammonia synthesis catalysts, *J. Am. Chem. Soc.*, 2001, **123**, 8404–8405.
- 46 X. Duan, J. Ji, G. Qian, C. Fan, Y. Zhu, X. Zhou, D. Chen and W. Yuan, Ammonia decomposition on Fe(110), Co(111) and Ni(111) surfaces: A density functional theory study, *J. Mol. Catal. A:Chem.*, 2012, **357**, 81–86.
- 47 D. P. Pathak, A. Kumar, B. M. Sivagnanam, A. S. K. Sinha and J. Karthikeyan, A DFT study of the ammonia decomposition mechanism on the electronically modified Fe<sub>3</sub>N surface by doping molybdenum, *J. Phys. Chem. C*, 2023, **127**, 16442–16452.
- 48 W. Zheng, T. P. Cotter, P. Kaghazchi, T. Jacob, B. Frank, K. Schlichte, W. Zhang, D. S. Su, F. Schüth and R. Schlögl, Experimental and theoretical investigation of molybdenum carbide and nitride as catalysts for ammonia decomposition, *J. Am. Chem. Soc.*, 2013, **135**, 3458–3464.
- 49 W. Guo and D. G. Vlachos, On factors controlling activity of submonolayer bimetallic catalysts: Nitrogen desorption, *J. Chem. Phys.*, 2014, **140**, 014703.
- 50 F. R. García-García, A. Guerrero-Ruiz and I. Rodríguez-Ramos, Role of B5-type sites in Ru catalysts used for the NH<sub>3</sub> decomposition reaction, *Top. Catal.*, 2009, **52**, 758–764.
- 51 X. Duan, G. Qian, X. Zhou, Z. Sui, D. Chen and W. Yuan, Tuning the size and shape of Fe nanoparticles on carbon nanofibers for catalytic ammonia decomposition, *Appl. Catal., B*, 2011, **101**, 189–196.
- 52 S. Chen, X. Chen and H. Zhang, Nanoscale size effect of octahedral nickel catalyst towards ammonia decomposition reaction, *Int. J. Hydrogen Energy*, 2017, **42**, 17122–17128.
- 53 L. Li, L. Zhao, Z. Ma, C. Li, J. Duan and W. Wang, Ce<sub>0.5</sub>Zr<sub>0.5</sub>O<sub>2</sub> solid solutions supported Co-Ni catalyst for ammonia oxidative decomposition to hydrogen, *Chem. Eng. J.*, 2023, **475**, 146355.
- 54 C. J. H. Jacobsen, S. Dahl, P. L. Hansen, E. Törnqvist, L. Jensen, H. Topsøe, D. V. Prip, P. B. Møenshaug and I. Chorkendorff, Structure sensitivity of supported ruthenium catalysts for ammonia synthesis, *J. Mol. Catal. A:Chem.*, 2000, **163**, 19–26.
- 55 M. El-Shafie, S. Kambara and Y. Hayakawa, Alumina particle size effect on H<sub>2</sub> production from ammonia decomposition by DBD plasma, *Energy Rep.*, 2020, **6**, 25–30.
- 56 J. Cha, T. Lee, Y. J. Lee, H. Jeong, Y. S. Jo, Y. Kim, S. W. Nam, J. Han, K. B. Lee, C. W. Yoon and H. Sohn, Highly monodisperse sub-nanometer and nanometer Ru particles confined in alkali-exchanged zeolite Y for ammonia decomposition, *Appl. Catal., B*, 2021, **283**, 119627.
- 57 H. Zhang, Y. A. Alhamed, Y. Kojima, A. A. Al-Zahrani, H. Miyaoka and L. A. Petrov, Structure and catalytic properties of Ni/MWCNTs and Ni/AC catalysts for hydrogen production via ammonia decomposition, *Int. J. Hydrogen Energy*, 2014, **39**, 277–287.
- 58 K. C. Leung, S. Hong, G. Li, Y. Xing, B. K. Y. Ng, P. L. Ho, D. Ye, P. Zhao, E. Tan, O. Safonova, T. S. Wu, M. M. J. Li, G. Mpourmpakis and S. C. E. Tsang, Confined Ru sites in a 13X zeolite for ultrahigh H<sub>2</sub> production from NH<sub>3</sub> decomposition, *J. Am. Chem. Soc.*, 2023, **145**, 14548–14561.
- 59 L. Yao, T. Shi, Y. Li, J. Zhao, W. Ji and C. T. Au, Core-shell structured nickel and ruthenium nanoparticles: Very active and stable catalysts for the generation of CO<sub>x</sub>-free hydrogen via ammonia decomposition, *Catal. Today*, 2011, **164**, 112–118.
- 60 A. Srifa, K. Okura, T. Okanishi, H. Muroyama, T. Matsui and K. Eguchi, Hydrogen production by ammonia decomposition over Cs-modified Co<sub>3</sub>Mo<sub>3</sub>N catalysts, *Appl. Catal., B*, 2017, **218**, 1–8.
- 61 Ł. Czekajło and Z. Lendzion-Bieluń, Effect of preparation conditions and promoters on the structure and activity of the ammonia decomposition reaction catalyst based on nanocrystalline cobalt, *Chem. Eng. J.*, 2016, **289**, 254–260.
- 62 W. Arabczyk and U. Narkiewicz, A new method for in situ determination of number of active sites in iron catalysts for ammonia synthesis and decomposition, *Appl. Surf. Sci.*, 2002, **196**, 423–428.
- 63 H. S. Zeng, K. Inazu and K. Aika, Dechlorination Process of active carbon-supported, barium nitrate-promoted ruthenium trichloride catalyst for ammonia synthesis, *Appl. Catal., A*, 2001, **219**, 235–247.
- 64 X. Ju, L. Liu, X. Zhang, J. Feng, T. He and P. Chen, Highly efficient Ru/MgO catalyst with surface-enriched basic sites for production of hydrogen from ammonia decomposition, *ChemCatChem*, 2019, **11**, 4161–4170.
- 65 C. Zheng, B. Guan, J. Guo, T. Su, J. Zhou, J. Chen, Y. Zhang, Y. Yuan, W. Xie, N. Zhou and Z. Huang, Research status, optimization strategies, and future prospects of ammonia decomposition catalysts for CO<sub>x</sub>-free hydrogen, *Ind. Eng. Chem. Res.*, 2023, **62**, 11305–11336.
- 66 W. Zhang, W. Zhou, Y. Li, J. Ren and Z. Wang, Enhanced ammonia decomposition activity over unsupported Co<sub>3</sub>O<sub>4</sub>: Unravelling the promotion effect of alkali metal, *Appl. Catal., B*, 2023, **330**, 122644.
- 67 X. Y. Guo, J. H. Wang, Q. Zhang, T. Z. Li, H. Dong, C. J. Jia, C. Li and Y. W. Zhang, Alkaline earth metal promoted hydrogen production from ammonia decomposition over Ni/La<sub>2</sub>O<sub>3</sub>-based catalysts, *Appl. Catal., B*, 2024, **348**, 123844.
- 68 L. Zhai, S. Liu and Z. Xiang, Ammonia as a carbon-free hydrogen carrier for fuel cells: A perspective, *Ind. Chem. Mater.*, 2023, **1**, 332–342.
- 69 J. Guo and P. Chen, Interplay of alkali, transition metals, nitrogen, and hydrogen in ammonia synthesis and decomposition reactions, *Acc. Chem. Res.*, 2021, **54**, 2434–2444.
- 70 J. G. Choi, Ammonia decomposition over vanadium carbide catalysts, *J. Catal.*, 1999, **182**, 104–116.
- 71 Z. Wang, Y. Qu, X. Shen and Z. Cai, Ruthenium catalyst supported on Ba modified ZrO<sub>2</sub> for ammonia decomposition to CO<sub>x</sub>-free hydrogen, *Int. J. Hydrogen Energy*, 2019, **44**, 7300–7307.



- 72 L. Torrente-Murciano, The importance of particle-support interaction on particle size determination by gas chemisorption, *J. Nanopart. Res.*, 2016, **18**, 87.
- 73 Z. Su, J. Guan, Y. Liu, D. Shi, Q. Wu, K. Chen, Y. Zhang and H. Li, Research progress of ruthenium-based catalysts for hydrogen production from ammonia decomposition, *Int. J. Hydrogen Energy*, 2024, **51**, 1019–1043.
- 74 L. Li, Z. H. Zhu, Z. F. Yan, G. Q. Lu and L. Rintoul, Catalytic ammonia decomposition over Ru/carbon catalysts: The importance of the structure of carbon support, *Appl. Catal., A*, 2007, **320**, 166–172.
- 75 W. Raróg-Pilecka, D. Szmigiel, Z. Kowalczyk, S. Jodzis and J. Zielinski, Ammonia decomposition over the carbon-based ruthenium catalyst promoted with barium or cesium, *J. Catal.*, 2003, **218**, 465–469.
- 76 T. Kocer, F. E. S. Oztuna, S. F. Kurtoglu, U. Unal and A. Uzun, Graphene aerogel-supported ruthenium nanoparticles for CO<sub>x</sub>-free hydrogen production from ammonia, *Appl. Catal., A*, 2021, **610**, 117969.
- 77 S. J. Wang, S. F. Yin, L. Li, B. Q. Xu, C. F. Ng and C. T. Au, Investigation on modification of Ru/CNTs catalyst for the generation of CO<sub>x</sub>-free hydrogen from ammonia, *Appl. Catal., B*, 2004, **52**, 287–299.
- 78 P. Liu, L. Sun, Z. Zhang, X. Wang, Y. Zhang and X. Yang, Hydrogen production from ammonia decomposition catalyzed by Ru nano-particles in alkaline molecular sieves under photothermal conditions, *Mol. Catal.*, 2023, **543**, 113160.
- 79 M. Pinzón, O. Avilés-García, A. R. de la Osa, A. de Lucas-Consuegra, P. Sánchez and A. Romero, New catalysts based on reduced graphene oxide for hydrogen production from ammonia decomposition, *Sustainable Chem. Pharm.*, 2022, **25**, 100615.
- 80 M. Pinzón, A. Romero, A. de Lucas Consuegra, A. R. de la Osa and P. Sánchez, Hydrogen production by ammonia decomposition over ruthenium supported on SiC catalyst, *J. Ind. Eng. Chem.*, 2021, **94**, 326–335.
- 81 W. Zheng, J. Zhang, H. Xu and W. Li, NH<sub>3</sub> decomposition kinetics on supported Ru clusters: Morphology and particle size effect, *Catal. Lett.*, 2007, **119**, 311–318.
- 82 H. Liu, Y. Zhang, S. Liu, S. Li and G. Liu, Ni-CeO<sub>2</sub> nanocomposite with enhanced metal-support interaction for effective ammonia decomposition to hydrogen, *Chem. Eng. J.*, 2023, **473**, 145371.
- 83 T. H. Ulucan, J. Wang, E. Onur, S. Chen, M. Behrens and C. Weidenthaler, Unveiling the structure–property relationship of MgO-supported Ni ammonia decomposition catalysts from bulk to atomic structure by in situ/operando studies, *ACS Catal.*, 2024, **14**, 2828–2841.
- 84 L. H. Yao, Y. X. Li, J. Zhao, W. J. Ji and C. T. Au, Core-shell structured nanoparticles (M@SiO<sub>2</sub>, Al<sub>2</sub>O<sub>3</sub>, MgO; M = Fe, Co, Ni, Ru) and their application in CO<sub>x</sub>-free H<sub>2</sub> production via NH<sub>3</sub> decomposition, *Catal. Today*, 2010, **158**, 401–408.
- 85 H. Muroyama, C. Saburi, T. Matsui and K. Eguchi, Ammonia decomposition over Ni/La<sub>2</sub>O<sub>3</sub> catalyst for on-site generation of hydrogen, *Appl. Catal., A*, 2012, **443–444**, 119–124.
- 86 K. Wu, C. F. Cao, C. Zhou, Y. Luo, C. Q. Chen, L. Lin, C. Au and L. Jiang, Engineering of Ce<sup>3+</sup>-O-Ni structures enriched with oxygen vacancies via Zr doping for effective generation of hydrogen from ammonia, *Chem. Eng. Sci.*, 2021, **245**, 116818.
- 87 C. Zhou, K. Wu, H. Huang, C. F. Cao, Y. Luo, C. Q. Chen, L. Lin, C. Au and L. Jiang, Spatial confinement of electron-rich Ni nanoparticles for efficient ammonia decomposition to hydrogen production, *ACS Catal.*, 2021, **11**, 10345–10350.
- 88 C. Chen, X. Fan, C. Zhou, L. Lin, Y. Luo, C. Au, G. Cai, X. Wang and L. Jiang, Hydrogen production from ammonia decomposition over Ni/CeO<sub>2</sub> catalyst: Effect of CeO<sub>2</sub> morphology, *J. Rare Earths*, 2023, **41**, 1014–1021.
- 89 H. Zhang, Y. A. Alhamed, Y. Kojima, A. A. Al-Zahrani, H. Miyaoka and L. A. Petrov, Structure and catalytic properties of Ni/MWCNTs and Ni/AC catalysts for hydrogen production via ammonia decomposition, *Int. J. Hydrogen Energy*, 2014, **39**, 277–287.
- 90 S. F. Yin, B. Q. Xu, W. X. Zhu, C. F. Ng, X. P. Zhou and C. T. Au, Carbon nanotubes-supported Ru catalyst for the generation of CO<sub>x</sub>-free hydrogen from ammonia, *Catal. Today*, 2004, **93–95**, 27–38.
- 91 X. Ju, L. Liu, P. Yu, J. Guo, X. Zhang, T. He, G. Wu and P. Chen, Mesoporous Ru/MgO prepared by a deposition-precipitation method as highly active catalyst for producing CO<sub>x</sub>-free hydrogen from ammonia decomposition, *Appl. Catal., B*, 2017, **211**, 167–175.
- 92 S. B. Simonsen, D. Chakraborty, I. Chorkendorff and S. Dahl, Alloyed Ni-Fe nanoparticles as catalysts for NH<sub>3</sub> decomposition, *Appl. Catal., A*, 2012, **447–448**, 22–31.
- 93 D. C. Huang, C. H. Jiang, F. J. Liu, Y. C. Cheng, Y. C. Chen and K. L. Hsueh, Preparation of Ru-Cs catalyst and its application on hydrogen production by ammonia decomposition, *Int. J. Hydrogen Energy*, 2013, **38**, 3233–3240.
- 94 S. F. Yin, B. Q. Xu, C. F. Ng and C. T. Au, Nano Ru/CNTs: A highly active and stable catalyst for the generation of CO<sub>x</sub>-free hydrogen in ammonia decomposition, *Appl. Catal., B*, 2004, **48**, 237–241.
- 95 S. F. Yin, Q. H. Zhang, B. Q. Xu, W. X. Zhu, C. F. Ng and C. T. Au, Investigation on the catalysis of CO<sub>x</sub>-free hydrogen generation from ammonia, *J. Catal.*, 2004, **224**, 384–396.
- 96 J. Chen, Z. H. Zhu, S. Wang, Q. Ma, V. Rudolph and G. Q. Lu, Effects of Nitrogen doping on the structure of carbon nanotubes (CNTs) and activity of Ru/CNTs in ammonia decomposition, *Chem. Eng. J.*, 2010, **156**, 404–410.
- 97 I. Nakamura and T. Fujitani, Role of metal oxide supports in NH<sub>3</sub> decomposition over Ni catalysts, *Appl. Catal., A*, 2016, **524**, 45–49.
- 98 C. Liang, W. Li, Z. Wei, Q. Xin and C. Li, Catalytic decomposition of ammonia over nitrided MoN<sub>x</sub>/α-Al<sub>2</sub>O<sub>3</sub> and NiMoN<sub>y</sub>/α-Al<sub>2</sub>O<sub>3</sub> catalysts, *Ind. Eng. Chem. Res.*, 2000, **39**, 3694–3697.



- 99 Y. Q. Gu, Z. Jin, H. Zhang, R. J. Xu, M. J. Zheng, Y. M. Guo, Q. S. Song and C. J. Jia, Transition metal nanoparticles dispersed in an alumina matrix as active and stable catalysts for CO<sub>x</sub>-free hydrogen production from ammonia, *J. Mater. Chem. A*, 2015, **3**, 17172–17180.
- 100 D. Rein, K. F. Ortega, C. Weidenthaler, E. Bill and M. Behrens, The roles of Co-precipitation pH, phase-purity and alloy formation for the ammonia decomposition activity of Ga-promoted Fe/MgO catalysts, *Appl. Catal., A*, 2017, **548**, 52–61.
- 101 Y. Q. Gu, Z. Jin, H. Zhang, R. J. Xu, M. J. Zheng, Y. M. Guo, Q. S. Song and C. J. Jia, Transition metal nanoparticles dispersed in an alumina matrix as active and stable catalysts for CO<sub>x</sub>-free hydrogen production from ammonia, *J. Mater. Chem. A*, 2015, **3**, 17172–17180.
- 102 J. Zhang, J. O. Müller, W. Zheng, D. Wang, D. Su and R. Schlögl, Individual Fe–Co alloy nanoparticles on carbon nanotubes: Structural and catalytic properties, *Nano Lett.*, 2008, **8**, 2738–2743.
- 103 J. Ji, X. Duan, G. Qian, X. Zhou, G. Tong and W. Yuan, Towards an efficient CoMo/ $\gamma$ -Al<sub>2</sub>O<sub>3</sub> catalyst using metal amine metallate as an active phase precursor: Enhanced hydrogen production by ammonia decomposition, *Int. J. Hydrogen Energy*, 2014, **39**, 12490–12498.
- 104 X. Wang, L. Li, Z. Fang, Y. Zhang, J. Ni, B. Lin, L. Zheng, C. Au and L. Jiang, Atomically dispersed Ru catalyst for low-temperature nitrogen activation to ammonia via an associative mechanism, *ACS Catal.*, 2020, **10**, 9504–9514.
- 105 S. M. Ghoreishian, K. Shariati, Y. S. Huh and J. Lauterbach, Recent advances in ammonia synthesis over ruthenium single-atom-embedded catalysts: A focused review, *Chem. Eng. J.*, 2023, **467**, 143533.
- 106 N. Shimoda, R. Yoshimura, T. Nukui and S. Satokawa, Alloying effect of nickel–cobalt based binary metal catalysts supported on  $\alpha$ -alumina for ammonia decomposition, *J. Chem. Eng. Jpn.*, 2019, **52**, 413–422.
- 107 X. Duan, G. Qian, X. Zhou, Z. Sui, D. Chen and W. Yuan, Tuning the size and shape of Fe nanoparticles on carbon nanofibers for catalytic ammonia decomposition, *Appl. Catal., B*, 2011, **101**, 189–196.
- 108 A. H. Lu, J. J. Nitz, M. Comotti, C. Weidenthaler, K. Schlichte, C. W. Lehmann, O. Terasaki and F. Schüth, Spatially and size selective synthesis of Fe-based nanoparticles on ordered mesoporous supports as highly active and stable catalysts for ammonia decomposition, *J. Am. Chem. Soc.*, 2010, **132**, 14152–14162.
- 109 T. E. Bell, H. Ménard, J. M. González Carballo, R. Tooez and L. Torrente-Murciano, Hydrogen production from ammonia decomposition using Co/ $\gamma$ -Al<sub>2</sub>O<sub>3</sub> catalysts – Insights into the effect of synthetic method, *Int. J. Hydrogen Energy*, 2020, **45**, 27210–27220.
- 110 B. Lorenzut, T. Montini, M. Bevilacqua and P. Fornasiero, FeMo-Based catalysts for H<sub>2</sub> production by NH<sub>3</sub> decomposition, *Appl. Catal., B*, 2012, **125**, 409–417.
- 111 L. A. Parker, N. Richards, L. Bailey, J. H. Carter, E. Nowicka, S. Pattison, N. F. Dummer, Q. He, L. Lu, C. J. Kiely, S. E. Golunski, A. Roldan and G. J. Hutchings, Investigating periodic table interpolation for the rational design of nanoalloy catalysts for green hydrogen production from ammonia decomposition, *Catal. Lett.*, 2023, **154**, 1958–1969.
- 112 H. Silva, M. G. Nielsen, E. M. Fiordaliso, C. D. Damsgaard, C. Gundlach, T. Kasama, I. B. Chorkendorff and D. Chakraborty, Synthesis and characterization of Fe–Ni/ $\gamma$ -Al<sub>2</sub>O<sub>3</sub> egg-shell catalyst for H<sub>2</sub> generation by ammonia decomposition, *Appl. Catal., A*, 2015, **505**, 548–556.
- 113 Z. Lendzion-Bieluń and W. Arabczyk, Fused FeCo catalysts for hydrogen production by means of the ammonia decomposition reaction, *Catal. Today*, 2013, **212**, 215–219.
- 114 A. Srifa, K. Okura, T. Okanishi, H. Muroyama, T. Matsui and K. Eguchi, CO<sub>x</sub>-free hydrogen production via ammonia decomposition over molybdenum nitride-based catalysts, *Catal. Sci. Technol.*, 2016, **6**, 7495–7504.
- 115 K. G. Kirste, K. McAulay, T. E. Bell, D. Stoian, S. Laassiri, A. Daisley, J. S. J. Hargreaves, K. Mathisen and L. Torrente-Murciano, CO<sub>x</sub>-free hydrogen production from ammonia – mimicking the activity of Ru catalysts with unsupported Co–Re alloys, *Appl. Catal., B*, 2021, **280**, 119405.
- 116 Z. Li, S. Ji, Y. Liu, X. Cao, S. Tian, Y. Chen, Z. Niu and Y. Li, Well-defined materials for heterogeneous catalysis: From nanoparticles to isolated single-atom sites, *Chem. Rev.*, 2019, **120**, 623–682.
- 117 W. Guo and D. G. Vlachos, Effect of local metal microstructure on adsorption on bimetallic surfaces: Atomic nitrogen on Ni/Pt(111), *J. Chem. Phys.*, 2013, **138**, 174702.
- 118 W. Guo and D. G. Vlachos, Patched bimetallic surfaces are active catalysts for ammonia decomposition, *Nat. Commun.*, 2015, **6**, 8619.
- 119 H. Wu, C. Liu and W. Guo, Computational screening of bimetallic catalysts: Application to ammonia decomposition, *J. Phys. Chem. C*, 2021, **126**, 192–202.
- 120 Y. Yao, Z. Liu, P. Xie, Z. Huang, T. Li, D. Morris, Z. Finrock, J. Zhou, M. Jiao, J. Gao, Y. Mao, J. Miao, P. Zhang, R. Shahbazian-Yassar, C. Wang, G. Wang and L. Hu, Computationally aided, entropy-driven synthesis of highly efficient and durable multi-elemental alloy catalysts, *Sci. Adv.*, 2020, **6**, eaaz0510.
- 121 E. P. George, D. Raabe and R. O. Ritchie, High-entropy alloys, *Nat. Rev. Mater.*, 2019, **4**, 515–534.
- 122 P. Xie, Y. Yao, Z. Huang, Z. Liu, J. Zhang, T. Li, G. Wang, R. Shahbazian-Yassar, L. Hu and C. Wang, Highly efficient decomposition of ammonia using high-entropy alloy catalysts, *Nat. Commun.*, 2019, **10**, 4011.
- 123 W. A. Saidi, W. Shadid and G. Veser, Optimization of high-entropy alloy catalyst for ammonia decomposition and ammonia synthesis, *J. Phys. Chem. Lett.*, 2021, **12**, 5185–5192.
- 124 K. Omata, K. Sato, K. Nagaoka, H. Yukawa, Y. Matsumoto and T. Nambu, Direct high-purity hydrogen production from ammonia by using a membrane reactor combining V-10mol%Fe hydrogen permeable alloy membrane with Ru/





- Cs<sub>2</sub>O/Pr<sub>6</sub>O<sub>11</sub> ammonia decomposition catalyst, *Int. J. Hydrogen Energy*, 2022, **47**, 8372–8381.
- 125 F. R. García-García, Y. H. Ma, I. Rodríguez-Ramos and A. Guerrero-Ruiz, High purity hydrogen production by low temperature catalytic ammonia decomposition in a multifunctional membrane reactor, *Catal. Commun.*, 2008, **9**, 482–486.
  - 126 J. Liu, X. Ju, C. Tang, L. Liu, H. Li and P. Chen, High performance stainless-steel supported Pd membranes with a finger-like and gap structure and its application in NH<sub>3</sub> decomposition membrane reactor, *Chem. Eng. J.*, 2020, **388**, 124245.
  - 127 N. Itoh, Y. Kikuchi, T. Furusawa and T. Sato, Tube-wall catalytic membrane reactor for hydrogen production by low-temperature ammonia decomposition, *Int. J. Hydrogen Energy*, 2021, **46**, 20257–20265.
  - 128 M. Guler, C. Korkusuz and D. Varisli, Catalytic decomposition of ammonia for hydrogen production over carbon nanofiber supported Fe and Mo catalysts in a microwave heated reactor, *Int. J. Chem. React. Eng.*, 2019, **17**, 20180162.
  - 129 R. Can Seyfeli and D. Varisli, Ammonia decomposition reaction to produce CO<sub>x</sub>-free hydrogen using carbon supported cobalt catalysts in microwave heated reactor system, *Int. J. Hydrogen Energy*, 2020, **45**, 34867–34878.
  - 130 J. A. Andersen, J. M. Christensen, M. Østberg, A. Bogaerts and A. D. Jensen, Plasma-catalytic ammonia decomposition using a packed-bed dielectric barrier discharge reactor, *Int. J. Hydrogen Energy*, 2022, **47**, 32081–32091.
  - 131 V. Cechetto, L. Di Felice, R. G. Martinez, A. A. Plazaola and F. Gallucci, Ultra-pure hydrogen production via ammonia decomposition in a catalytic membrane reactor, *Int. J. Hydrogen Energy*, 2022, **47**, 21220–21230.
  - 132 O. Elishav, D. R. Lewin, G. E. Shter and G. S. Grader, The nitrogen economy: Economic feasibility analysis of nitrogen-based fuels as energy carriers, *Appl. Energy*, 2017, **185**, 183–188.
  - 133 L. Wang, Y. Yi, Y. Zhao, R. Zhang, J. Zhang and H. Guo, NH<sub>3</sub> decomposition for H<sub>2</sub> generation: Effects of cheap metals and supports on plasma-catalyst synergy, *ACS Catal.*, 2015, **5**, 4167–4174.
  - 134 M. Saryer, A. A. Bozdağ, N. A. Sezgi and T. Doğu, Performance comparison of microwave and conventionally heated reactors for sorption enhanced reforming of ethanol over Ni impregnated SBA-15, *Chem. Eng. J.*, 2019, **377**, 120138.
  - 135 Y. Hayakawa, T. Miura, K. Shizuya, S. Wakazono, K. Tokunaga and S. Kambara, Hydrogen production system combined with a catalytic reactor and a plasma membrane reactor from ammonia, *Int. J. Hydrogen Energy*, 2019, **44**, 9987–9993.
  - 136 Z. N. Yildiz and D. Varisli, Conversion of ammonia to hydrogen in the microwave reactor system using Mo@alumina catalysts with the promotion of rare-earth and alkaline earth elements, *Renewable Energy*, 2024, **228**, 120603.
  - 137 M. El-Shafie, S. Kambara and Y. Hayakawa, Alumina particle size effect on H<sub>2</sub> production from ammonia decomposition by DBD plasma, *Energy Rep.*, 2020, **6**, 25–30.
  - 138 M. El-Shafie, S. Kambara and Y. Hayakawa, Plasma-enhanced catalytic ammonia decomposition over ruthenium (Ru/Al<sub>2</sub>O<sub>3</sub>) and soda glass (SiO<sub>2</sub>) materials, *J. Energy Inst.*, 2021, **99**, 145–153.
  - 139 L. Wang, Y. Zhao, C. Liu, W. Gong and H. Guo, Plasma driven ammonia decomposition on a Fe-catalyst: Eliminating surface nitrogen poisoning, *Chem. Commun.*, 2013, **49**, 3787.
  - 140 Y. Zhao, L. Wang, J. Zhang and H. Guo, Enhancing the ammonia to hydrogen (ATH) energy efficiency of alternating current arc discharge, *Int. J. Hydrogen Energy*, 2014, **39**, 7655–7663.
  - 141 Q. F. Lin, Y. M. Jiang, C. Z. Liu, L. W. Chen, W. J. Zhang, J. Ding and J. G. Li, Instantaneous hydrogen production from ammonia by non-thermal arc plasma combining with catalyst, *Energy Rep.*, 2021, **7**, 4064–4070.

